NASA Technical Memorandum 88993

ADVANCED TURBOPROP NOISE
PREDICTION-DEVELOPMENT OF
A CODE AT NASA LANGLEY BASED
ON RECENT THEORETICAL RESULTS

F. FARASSAT, MARK H. DUNN,
AND SHARON L. PADULA

JULY 1986

FOR REFERENCE

NASA

National Aeronautics and
Space Administration

Langley Research Center
Hampton, Virginia 23665

INTRODUCTION

Advanced turboprops are highly loaded propellers with blades that are swept back and run at supersonic tip speed in cruise condition. Many studies have shown that the efficiency of advanced turboprops is higher than the current turbofan designs [1]. In fact, if the technological problems associated with the design and manufacture of these turboprops are overcome and they get into airline service, the fuel saving compared to today's airliners will be substantial. The current prototype designs employ one or two rows (contra-rotating) of blades, Fig. 1. One major design problem is the prediction of discrete frequency noise of these propellers. This prediction is required to reduce both the cabin interior noise and the impact on the community around airports.

The availability of high speed computers with large memory has made it possible to use sophisticated realistic modelling which involves substantial data handling. One of the most useful tools of noise prediction is the acoustic analogy [2]. Noise prediction procedures based on the acoustic analogy require the blade surface pressure data in addition to propeller geometric and kinematic data as input. Thus a typical procedure utilizes several major prediction codes such as propeller aerodynamics, propeller acoustics and codes which model other physical effects such as fuselage scattering or boundary layer propagation. Development and verification of each of these codes is time consuming and expensive.

This paper describes a computer code for advanced propeller noise prediction developed at NASA Langley Research Center and based on recent theoretical work on acoustics of high speed sources. The computation is in time domain resulting in acoustic pressure signature which is then Fourier analyzed to obtain the acoustic spectrum of the noise. The blades are divided into panels and the contribution of each panel to the overall noise of the propeller is evaluated individually. Two acoustic formulations are used in the code. The code selects one of the

two formulations depending on the value of the Doppler factor at the emission time of a blade panel.

The entire process of propeller noise prediction is described in the first two sections of this paper which cover theory and implementation. Several examples of applications of this program are given in a section on comparison with measured data. These examples show some of the capabilities of the code. In the appendix, the two formulations used in the code are briefly derived.

In the last decade, several computer codes for prediction of the discrete frequency noise of helicopter rotors and propellers have been developed at NASA Langley [3]. The two comprehensive noise prediction codes of NASA, ANOPP (see [4] for propellers) and ROTONET (helicopter rotors), incorporate acoustic formulas after they are verified by researchers. The code reported here is a stand-alone program which differs from the present ANOPP discrete frequency noise module in using a more recent high speed source formulation. It is built on the experience gained in development of other codes at Langley.

THEORETICAL FORMULATIONS

The two formulations used in the coding are the solutions of the Ffowcs Williams-Hawkings (FW-H) equation with thickness and loading source terms only. Because of the thin blades of the current advanced propeller designs, quadrupole noise is believed to be small compared to thickness and loading noise [5]. Hence this noise is not included in prediction. However, the authors do not claim that the nonlinear effects are entirely negligible for advanced propellers. Rather, a careful evaluation of the effectiveness of the present code is recommended. Following that, the inclusion of nonlinear effects, perhaps without the use of the acoustic analogy, can be explored [6].

Experience in development of noise prediction codes at Langley has shown that no single solution of the FW-H equation is suitable for efficient calculation of propeller noise and for all ranges of tip Mach numbers of interest. For this reason at least two formulations are needed depending on the magnitude of the Doppler factor $1-M_r$. Here M_r is Mach number in the radiation direction. Each formulation must be valid for near and far field observer locations and must be efficiently coded to handle observers fixed to the ground frame or fixed to the aircraft frame. Moreover, full geometric modelling with minimum approximation of blade shape should be used in the coding. These criteria can be met easily by using time domain formulations. Since, many time domain formulations are possible [7], some care is required in selection of the best two for coding. One major advantage of using time domain method is that one does not need to develop separate results for the near and far fields.

In the code discussed here the two formulations used were derived and published elsewhere [8-10]. A very brief derivation of these results is presented in an appendix of this paper. The FW-H equation is written in the following form

$$\Box^2 p' = \frac{1}{c}\frac{\partial}{\partial t}\,[M_n|\nabla f|\delta(f)] - \nabla \cdot [p\underset{\sim}{n}|\nabla f|\delta(f)] = \nabla_4 \cdot [\underset{\sim}{Q}|\nabla f|\delta(f)] \qquad (1)$$

where p' is the nondimensional acoustic pressure, M_n is the local normal Mach number and c is the speed of sound in the undisturbed medium. The nondimensional blade surface pressure is p. Both p' and p are nondimensionalized with respect to $\rho_0 c^2$ where ρ_0 is the density of the undisturbed medium. The blade surface is described by $f(\underset{\sim}{x},t)=0$ and $\underset{\sim}{n}$ is the local unit outward normal. The 4-divergence ∇_4 is $(\nabla, 1/c\ \partial/\partial t)$ and $\underset{\sim}{Q}=(-p\underset{\sim}{n}, M_n)$.

When $M_r<1-\varepsilon$, where ε is a small positive number, the acoustic pressure is calculated by using the following expression whose full derivation is given in [8]

$$4\pi p_L'\,(\underset{\sim}{x},t) = \frac{1}{c}\int_{f=0}\left[\frac{\dot p\cos\theta}{r(1-M_r)^2}\right]_{ret}dS$$

$$+\int_{f=0}\left[\frac{p(\cos\theta-M_n)}{r^2(1-M_r)^2}\right]_{ret}dS$$

$$+\frac{1}{c}\int_{f=0}\left[\frac{p\cos\theta(r\dot M_i\hat r_i+cM_r-cM^2}{r^2(1-M_r)^3}\right]_{ret}dS \tag{2a}$$

$$4\pi p_T'\,(\underset{\sim}{x},t) = \frac{1}{c}\int_{f=0}\left[\frac{M_n(r\dot M_i\hat r_i+cM_r-cM^2}{r^2(1-M_r)^3}\right]_{ret}dS \tag{2b}$$

$$p'\,(\underset{\sim}{x},t) = p_L'\,(\underset{\sim}{x},t) + p_T'\,(\underset{\sim}{x},t) \tag{2c}$$

Here p_L' and p_T' stand for the acoustic pressure due to loading and thickness respectively. The dot on $\dot M_i$ and $\dot p$ denote rate of variation of these vectors with respect to the source time. The symbols have the usual meaning and are defined at the end of the paper. This result is referred to as Formulation 1-A.

When $M_r>1-\varepsilon$, Eq. (1) becomes useless because of the sensitivity of the integrals to errors and the singularity of the integrands when $\left|1-M_r\right|$ is small. The formulation used in an earlier version of the Langley code for high speed propellers (Farassat-Nystrom) is valid for all ranges of Mach numbers [3]. But the poor execution time on a computer and sensitivity to an observer time differentiation led to the derivation of a more suitable analytic result which was singularity-free for the range when $\left|1-M_r\right|$ is small. The detailed derivation of this result is in Ref. [9] with a briefer derivation in [10]. See also the appendix. The acoustic pressure is calculated using the following formula

$$4\pi p'(\underset{\sim}{x},t) = \int\limits_{\substack{F=0 \\ K>0}} \frac{1}{r^2} \left[\frac{1}{\Lambda} (p + M_n{}^2)Q_N'\right]d\Sigma$$

$$+ \int\limits_{\substack{F=0 \\ K>0}} \frac{1}{r} \left\{\frac{1}{\Lambda} \left[(p + M_n{}^2)Q_F + Q'_F + Q''_F]\right\}_{ret}d\Sigma$$

$$- \int\limits_{\substack{F=0 \\ K=0}} \frac{1}{r} \left\{\frac{1}{\Lambda_o} \left[(p + M_n{}^2)Q_E + M_n M_{av}]\right\}_{ret}d\gamma \tag{3}$$

This expression is written for an open surface (e.g. a panel on the blade) described by $f(\underset{\sim}{y},\tau)=0$ and $k(\underset{\sim}{y},\tau)>0$. As will be explained later, this result is used for panels for which $M_r>1-\epsilon$ for some specified value of ϵ. The first two integrals are surface integrals over the surface Σ: $F=0$ and $K>0$ where $F=[f(\underset{\sim}{y},\tau)]_{ret}$ and $K=[k(\underset{\sim}{y},\tau)]_{ret}$. The last integral is a line integral over the edge of surface Σ which is described by the equations $F=K=0$. Note that Q'_F depends on the local surface derivatives of the surface pressure p. Both Q'_F and Q''_F depend on the local principal curvatures of blade surface. To get the expression for the thickness noise p'_T from Eq. (3), drop all terms in the integrands involving p. The loading noise p'_L is then obtained by using $p'_L=p'-p'_T$.

A common approximation in noise prediction of propellers is using the mean surface of the blade in place of the actual blade (or the full) surface. The mean surface results will now be given since such an approximation is an option in the code reported here. To get the mean surface approximation of Eq. (2), replace p by $-\Delta p$ where $\Delta p=(p)_{lower}-(p)_{upper}$. Also replace M_n by $2\overline{M}_n$ where $2\overline{M}_n=(M_n)_{upper}+(M_n)_{lower}$. The surface integral is over the mean surface of blades described by the mean camber lines.

The mean surface approximation of Eq. (3) is not straightforward. One needs to start from the governing differential equation (FW-H) written with

sources on the mean surface [10]. The resulting expression for an open surface is

$$2\pi p_T'(\underset{\sim}{x},t) = \int\limits_{\substack{F_m=0 \\ K>0}} \frac{1}{r} \left[\frac{\overline{Q''}_F}{\Lambda}\right]_{ret} d\Sigma - \int\limits_{\substack{F_m=0 \\ K=0}} \frac{1}{r} \left[\frac{\overline{M}_n \underset{\sim}{M}_t \cdot \underset{\sim}{\nu}}{\Lambda}\right]_{ret} d\gamma \qquad (4a)$$

$$4\pi p_L'(\underset{\sim}{x},t) = -\int\limits_{\substack{F_m=0 \\ K>0}} \frac{1}{r^2} \left[\frac{\Delta p Q_N'}{\Lambda}\right]_{ret} d\Sigma + \int\limits_{\substack{F_m=0 \\ K>0}} \frac{1}{r} \left[\frac{1}{\Lambda} \left(b\frac{\partial \Delta p}{\partial \sigma_b} - \frac{\lambda}{c} \dot{\Delta p}\right)\right]_{ret} d\Sigma$$

$$+ \int\limits_{\substack{F_m=0 \\ K=0}} \frac{1}{r} \left[\frac{\Delta p b_\nu}{\Lambda_o}\right]_{ret} d\gamma \qquad , \qquad (4b)$$

In the next section the method of coding of these formulas on a computer is presented.

IMPLEMENTATION ON A COMPUTER

The first step in coding Eqs. (2), (3) and (4) is geometric modelling of the blades. The geometric modelling of the present code is similar to that of Ref. [3]. A blade is described in a Cartesian frame ($\underset{\sim}{\eta}$-frame) fixed to the blade as follows. The origin of the frame is at the intersection of the propeller axis and the blade pitch change axis. The three axes of the frame are taken at the propeller shaft axis (η_3), pitch change axis (η_2) and the η_1-axis is taken normal to $\eta_2\eta_3$-plane in such a way that the $\underset{\sim}{\eta}$-frame is right-handed. The chordwise direction is thus parallel to the $\eta_1\eta_3$-plane.

To specify the blade, the leading edge curve·of the blade is first defined as a function of radial distance η_2 along pitch change axis. The airfoil section shape and geometric angle of attack (pitch) is then specified at a number of radial stations. The blade shape is constructed by

laying the airfoil sections at their prescribed angle of attack and with their leading edges on the leading edge curve. Blade geometric parameters such as the unit normal and the principal curvatures are then calculated from this information. Blade geometric data can be specified analytically or as a table which may require interpolation to read into the computer code.

A simplified flow chart of the computer program is shown in Fig. 2. Before discussing some parts of the code in detail, a few remarks on the method of implementation on the computer will be made. The pressure signature of only one blade is calculated. The signature for several blades is calculated by shifting the signature for one blade in time as many times as the number of blades and summing the pressures for each observer time within a period (based on the blade passage frequency). The blade for which the noise is predicted is first divided into panels. To reduce memory requirement, the sound from one panel is calculated for one complete revolution of the blade and then the saved geometric data are discarded. Essentially, then Eqs. (2), (3) and (4) are used for panels only and decision must be made as to when Formulation 1-A or 3 must be used. This and some other details of the code will now be presented.

Division of the Blades into Panels

The blade is first divided into two portions by a chordwise cut where the helical Mach number is near unity (i.e.=1-ε). The input variable ε (usually taken as 0.05) determines the exact location of the cut below the sonic line. The reason for dividing the blade in this way is that for all the panels on the inner portion, only Formulation 1-A needs to be used while for some of the panels on the outer portion, Formulation 3 must be used. A coarse mesh is laid out on the upper and lower surfaces of the blade (or on the mean surface) as required. The mesh consists of lines in chordwise direction and curves of constant nondimensional distance from leading edge. Nondimensionalization of the distance from leading edge is with respect to the local chord. The general

shape of a panel is a parallelogram with two edges in chordwise direction. The remaining two edges are approximately parallel to the leading and trailing edge directions at the same radial position as the panel itself. See figure 3 for a typical panel shape. Provision is made to use different panel sizes for the inner and outer portions of the blade. If Formulation 3 is required for one panel (see below for criterion to select formulation), then that panel is further subdivided into smaller panels by exactly the procedure described above for generating the coarse mesh on the blade. Before the blade is divided into smaller panels, however, the line integrals (of Eq. (3) or Eq. (4)) over the edges are evaluated.

Emission Time Calculation

The emission time calculations are needed both in the acoustic calculation and the decision making process for formulation selection. The equation for finding the emission time is transcendental function of observer time and position. The equation can be written in such a way that the required emission times are the abscissas of the points of intersection of a parabola and a sinusoidal curve [3,4]. Development of a reliable code for this part of the program turned out to be very difficult. Indeed, several exceptional circumstances occur which require decision making and additional lines of coding. Considerable effort was spent to ensure all roots of the emission time equation were calculated. A numerical technique similar to that of references [3] and [4] was employed for solving this equation.

As an example of the precision of the present emission time routine, a particularly difficult case of finding the emission times of a small segment of the blade leading edge will be considered now. This segment which has both single and multiple emission times at the selected observer time, is moving at supersonic helical speed. Its operating condition is recorded in Table 1. The

SR-3 blade planform is used. Figure 4 shows the emission time (or times) versus distance along the edge. The emission times of about 100 points along this line segment were calculated for this plot at a single observer time. It is seen that the inboard portion of the line segment has a single emission time while the rest of the segment has three emission times. Note that the part of the curve that looks like a straight line has a small slope. The smoothness of these two pieces of curves in Fig. 4 which are not smoothed numerically is an indication of precision of the emission time routine.

Criterion for Selection of Formulation

An automatic decision making process must be used for each panel in the supersonic portion of the blade as to the type of Formulation (1-A or 3) for noise prediction. Since Gauss-Legendre integration is used exclusively for Formulation 1-A, i.e., for subsonic panels, the nodes for Gauss-Legendre (G-L) integration are first determined for each coarse panel as shown in Fig. 3b. The number of these nodes can be specified from 9(3×3) to 100(10×10). If a node on a panel has multiple emission time, Formulation 3 is used for that panel. Only if all nodes have single emission time and if $M_r < 1-\epsilon$ at each node at its emission time, then Formulation 1-A is used. Formulation 3 is used as follows. The coarse-sized panel is divided into smaller fine-sized panels. Equation (3) is used by replacing $d\Sigma/\Lambda$ by $cd\tau d\Gamma/\sin\theta$ from Eq. (A8). This kind of integration over the Σ-surface is known as the collapsing sphere method. Again considerable care is required to extend the source time integration to capture all the Σ-surface area of a panel. In particular, this surface can be more than one piece and all the pieces must be included in integration.

Figure 5 shows panels for which Formulation 3 is used at three observer times marked on the pressure signature also shown in the figure. The signature is for one blade only. The panels shown are the coarse panels introduced

above. In a typical calculation, the coarse panel size is generally much larger than those shown in Fig. 5. For completeness, it is mentioned that the operating conditions used in this figure corresponds to Table 1 and the observer position is at microphone 4 (see Table 2).

Motion of the Observer

The acoustic equations of this paper are derived in the frame fixed to the medium. That is $\underset{\sim}{x}$ in $p'(\underset{\sim}{x},t)$ is in the ground-fixed frame. If $\underset{\sim}{\bar{x}}$ is the observer variable in the frame fixed to the aircraft moving at steady forward velocity $\underset{\sim}{V_F}$, then

$$p'(\underset{\sim}{\bar{x}},t) = p'(\underset{\sim}{x}_0 + \underset{\sim}{V_F}t,\ t) \tag{5}$$

where $\underset{\sim}{x}_0$ is the observer position in the ground-fixed frame at time t=0. This transformation is used to find the acoustic waveform in the moving frame.

Unsteady Loading Noise

The unsteady loading noise is calculated by specifying the blade surface pressure p as a function of time in the input data. The rate of change of the surface pressure with respect to time, p, must be calculated from p. Both of the formulations used here (1-A and 3) have a term involving p. It must be noted that interpolations in surface variables and time of p are required to evaluate the integrands of the acoustic results. Obviously, more time is spent on the computer for unsteady blade loading than for the steady case.

Contra-rotating Propellers

The prediction of the noise of contra-rotating propellers can be accomplished as follows. For a single rotor, the observer location is specified in a frame whose origin is at the disk center (i.e. where the pitch

change axis intersects the propeller axis). For contra-rotating propellers, two
sets of calculations must be performed with the observer specified at correct
position in the frame of each rotor. It must be mentioned that the observer
time origin (time t=0) is the same in all frames so that simple superposition of
pressure signatures from each rotor gives the overall acoustic pressure
signature.

The Output Data

The acoustic pressure signature of one blade for period T corresponding to
one complete revolution, is calculated first. For B blades, this signature is
shifted by T/B seconds for B times. The overall acoustic signature for B blades
is the sum of the signatures over any length of time of duration T/B. Following
this, discrete Fourier analysis is used to obtain the acoustic spectrum.

COMPUTATIONAL GRID SIZE STUDY AND COMPARISON WITH AN EARLIER LANGLEY CODE

As mentioned in the previous section, the initial step in the computation
is segmenting the blade surface into coarse size panels. If Formulation 3 is to
be used for a panel, further subdivision into fine size panels is made. Too
large a panel size results in computational errors while too fine a panel size
results in excessive computer time. Furthermore, since Formulation 3 uses more
time to execute on a computer than Formulation 1-A, because of the total number
of operations needed per observer time, it is desirable to reduce the number of
panels using Formulation 3. This is conntrolled by the size of the parameter
ε. In this section the effects of grid size and ε are studied on the execution
time and on the acoustic pressure signature and spectrum. In addition, the
consistency of Formulations 1-A and 3 versus Eormulation 1 used in
Nystrom-Farassat code [3] is established in this section.

All the data presented are for the demanding case of an advanced propeller with swept blades (SR-3). The blade planform is shown in Fig. 3. The blade form curves were shown in reference [3]. The operating conditions and some design data are presented in Table 1. The operating conditions pertain to a flight test in which the propeller was flown on a pylon fixed on the top of the fuselage of a jet powered aircraft. The microphones were mounted on a boom held above the propeller, Fig. 6. The microphone positions are given in Table 2. Because of a malfunction in the test, microphone number 2 data are ignored. In the discussions of this section all calculations are for microphone 4 which is behind the propeller disk. This position is chosen because during development of the code more difficulties were encountered here than the other two microphone positions. All predictions are performed using the full surface results of Formulations 1-A and 3. The blade surface pressure was obtained from a code using Denton's scheme [11]. Figure 7a and b shows the distribution of the upper and the lower pressure on the blade, respectively, in perspective. Note that the vertical scale is the pressure and the computational (rather than the physical) grid system is used for chordwise and spanwise direction. The blade sweep is, therefore, not shown in this figure. Figure 7c and d shows the same data in contour plot form.

Four grid sizes were selected as shown in Table 3. Grids A, B, and C refer to those coarse panels shown in Fig. 8. The fine grid refers to division of coarse panels, i.e., 10×10 means that a coarse sized panel is further divided into 10 equal chordwise and 10 equal spanwise divisions. The value of ε is taken as 0.05 and a 7×7 Gauss-Legendre integration scheme (for Formulation 1-A) is used in all calculations. In the Table 3, the relative cost of execution on a computer is also given. The execution time of grid system 3 was assumed as the unit time for the study of relative computation time. This grid system appears to be the best for noise prediction based on the present code. Table 4

shows the acoustic pressure spectra (re: 20µPa) for the noise components and the overall sound pressure level at microphone 4 for the four grid systems of Table 3. Figure 9 shows the corresponding acoustic pressure signatures. It is assumed that the smallest grid system 4 is the most accurate of all calculations and therefore it is used to evaluate other grid sizes.

Grid system 1 gives quite poor OASPL and spectrum. Also the acoustic pressure signature is considerably different from figure 9(d). For this reason, system 1 is judged unacceptable. Grid system 2 gives a good OASPL. The first 9 harmonics are within 2 dB and several of the harmonics are within 1 dB of those of grid system 4. The acoustic pressure signature shows noticeable similarity with that of grid system 4 but is much less smooth. This grid system is judged acceptable if only the first few harmonics are required. Grid system 3 gives a good OASPL. The acoustic spectrum agrees within 1 dB of that of grid system 4 up to 11th harmonics and for the remaining harmonics, the agreement is within 2 dB. The acoustic pressure signature with minor differences is also very similar to that of grid system 4. In view of the above results and the much lower execution time for grid system 3 as compared to grid system 4, the former grid is judged as the one most suitable for noise calculations.

The next study is on the selection of the value of ε which determines the choice of formulation for panels. In this connection, it must be mentioned that the numerical line and surface integration schemes used in Formulation 3 are less accurate than Gauss-Legendre scheme used in Formulation 1-A. Also as mentioned earlier, small ε is favored to reduce execution time. However, because of the large size of panels used in the latter case, there is the possibility of missing regions of multiple emission time for these panels if ε is too small. This is because of the discrete nature of the criterion for selection of formulation.

Three values of ε were assumed for this study, 0.05, 0.1 and 0.2. Grid system 3, Table 3, was used for all calculations. Compared to $\varepsilon=0.05$, the

relative execution times for $\epsilon=0.1$ and 0.2 are 1.04 and 1.31 respectively. Table 5 shows the acoustic spectra at microphone 4 for $\epsilon=0.1$ and 0.2. Case $\epsilon=0.05$ is shown in Table 4 and is used as reference for comparison. The acoustic pressure signatures corresponding to Table 5 are shown in Fig. 10. It is seen that the OASPL of all the cases are within 0.1 dB of each other. For $\epsilon=0.05$ and 0.1 the acoustic spectra are within 0.5 dB up to 11th harmonic. Thereafter, deviation of up to 2 dBs are observed but in most cases deviations are smaller. Comparing cases $\epsilon=0.05$ and 0.2, it is seen that the acoustic spectra are within 0.5 dB up to 7th harmonic and the remaining harmonics are within 1 dB deviation. The acoustic pressure signatures for the three cases look very similar in detail. Case $\epsilon=0.05$ was selected to reduce computation time.

The output of the present code is now compared to that of an earlier code (Nystrom-Farassat) of NASA Langley. Identical input data were used in the two runs. The aerodynamics input data to both codes, however, is similar to that of Ref. [3] with appropriate correction for horsepower. The full surface option of the codes were used. Figure 11 shows the acoustic pressure signatures and spectra for microphone 4. One striking difference is the high frequency oscillations due to numerical errors seen in the signatures of the old code. However, it is obvious that the signatures have quite similar characters. The acoustic pressure spectra, except for higher harmonics, are also very similar. The deviations in high harmonics are caused by numerical errors of the old code. Comparing the results of both codes, it is obvious that the new code introduces an improvement over the old code. One major advantage of the present code is that in this example the execution time was about 5 times faster than Nystrom-Farassat code.

COMPARISON WITH MEASURED DATA

In this section the theoretical prediction from the present code is compared with measured data for the test discussed in the preceeding section. Both the wave forms and acoustic spectra are used for comparison. It is very difficult to find experimental propeller acoustic data which is not contaminated by other physical effects such as reflections from hard surfaces nearby and fuselage boundary layer propagation. Thus, the present noise prediction code should be supplemented with other codes to include additional physical effects observed in the experiments. It was not possible to include quantitatively these effects with precision in the cases presented here. The sources of error are pointed out where they could be identified.

Before presenting the results of the calculations, two comments on the aerodynamic input data, Fig. 7, and boom reflection correction are in order. The original aerodynamic prediction code underestimated the absorbed power by about 25 percent. The source of this problem is thought to be related to the viscous flow phenomena in the inboard region of the blades. For this reason the predicted blade surface pressure was corrected by multiplying it by a linear function of radial position which decreased to the value of one at the tip. The required slope of this function is actually very small. Although the pressure distribution of Fig. 7 seems reasonable, some numerical experiments with the present acoustic code have shown that perhaps the actual chordwise distribution in the outboard region of the blades in the test is different from predicted. This point can not be verified since experimental blade surface pressure data are very rare.

The microphones used in the test were flush mounted on the boom and were 1/8 inch in diameter. The influence of the boom on microphone measurements can be estimated using the results of Morse [12] on scattering from cylinders. However, the estimation requires some approximations whose influence on the

estimation cannot be ascertained. One of these approximations is the direction of propagation of sound, which because of proximity of the source and microphones cannot be determined. It was, therefore, thought reasonable to take a correction of 4 dB for all microphones and all the harmonics of the spectra. Similarly, predicted acoustic pressure signatures were multiplied by the factor 1.58. This was the correction suggested and used by Brooks and Mackall [13]. It is known that this correction is a function of frequency [12]. The proposed correction must therefore be regarded as approximate. In fact, the estimation of what the microphones measure is very difficult because of the nature of the source (distributed), refraction of the sound in the fuselage boundary layer and its subsequent reflection from fuselage surface. The solution of such problems requires development of other computer codes.

Figure 12 shows the measured and predicted acoustic pressure signatures and spectra for microphone 1. The measured and predicted signatures are similar but there is an overprediction. Similar trend is seen in spectra also. Prediction based on Hanson's method for one harmonic from [13] agrees well with prediction from present code. No information on assumed blade loads is given in reference [13]. It is known that in Hanson's method the thickness and loading sources are located on a helicoidal surface which is infinitely thin. Quadrupole sources were also used in acoustic calculations of reference [13] but they make only a small contribution. It is interesting to note that this boom microphone is significantly influenced by the presence of the fuselage. A measure of this influence can be obtained by using an image propeller symmetrically located with respect to the tangent plane at the point where the radial line joining the fuselage center and propeller center meets the fuselage. Figure 13 shows this arrangement.

Figure 14 shows the corrected acoustic pressure signature and spectrum of the image propeller at microphone 1. It is seen that the image propeller alone generates as much noise as is measured by the microphone. Of course, refraction

through fuselage boundary layer and fuselage curvature effect on reflection are not included in this study. Nevertheless, this study shows that propeller noise measured at the boom microphone 1 is highly contaminated by the presence of the fusealge. This effect does not appear to be as significant for the other two microphone positions although the signatures seem to show this effect to some extent. Figure 15 shows the corrected acoustic pressures and spectra of the image propeller at microphones 3 and 4.

Figure 16 shows the predicted and measured acoustic pressure signatures and spectra for microphone 3. The predicted acoustic pressure signature is very similar to measured signature. A sharp positive peak in predicted signature is most likely wiped out in measurement due to the finite size of the microphone. The need for microphone size correction in another situation is discussed by Atvars et al [14]. The removal of this peak reduces the high harmonics of predicted spectrum and improves the agreement between measured and predicted spectra. The first three harmonics and the fifth harmonic are within 2 dB of measurement. Considering the fuselage reflection and boom effects, the agreement between the two spectra is good. Prediction of first harmonic based on Hanson's method [13] agrees slightly better than the present method perhaps due to differences in input data.

Figure 17 shows the measured and predicted acoustic pressure signature and spectra for boom microphone 4. The measured signature has the general features but is much broader near the negative peak than predicted waveform. A different blade chordwise surface pressure in the outboard region can explain this difference. For example, if the theoretical parabolic type chordwise distribution in the outboard region of the blade is replaced by a linear one peaking at the leading edge, then a signature with broader negative peak is obtained. Also fuselage reflection can affect the shape of the signature. This has not been included in prediction. The predicted spectrum underestimates the

first, fourth and fifth harmonics but the general trend of prediction is good. The first harmonic about 2 dB below prediction by Hanson's method [13].

So far all predictions presented here use the full surface results. Figure 18 shows the predicted acoustic pressure signature and spectra for microphone 4 using the mean surface results. The measured spectrum is also included for comparison. The surface pressure was obtained from the same aerodynamic code which gave the result shown in Fig. 7. The correction for power absorbed discussed earlier was also used. The predicted acoustic signature and spectrum using full surface result are essentially similar to those of mean surface. The signature from full surface code (Fig. 17) has a higher positive peak but other differences appear to be minute. However, a careful study of the predicted spectra from mean and full surface codes shows that the latter generally agrees better with the measured spectrum. Similar trend has been observed in the past. This is one reason for developing the full surface code even if execution time on a computer is longer than the mean surface code. The prediction of first harmonic by Hanson's method [13], which is based on a mean surface result, is again higher than the current code as seen in Fig. 18. Again the effect of differences in input data cannot be assessed.

CONCLUDING REMARKS

This paper presents the development of a computer code for prediction of the noise of high speed propellers. This code is based on two recent acoustic formulations, each of which is suitable for a different range of the Doppler factor of the sources on the blades. The use of these formulations plus improvements in algorithms employed in coding have resulted in great increase in accuracy and speed of execution on a computer.

It must be mentioned that this code should be supplemented by other aerodynamic and acoustic codes (e.g. boundary layer refraction, atmospheric propagation, ground effects and fuselage reflection) for prediction of the noise of a propeller in realistic cases. As such the development of the present code is just one step in designing a sophisticated multi-module propeller noise prediction program which includes all the physical phenomena existing in actual flight conditions.

One use of the code which has not been emphasized earlier is for structural acoustic purposes. Some of the recent fuselage propagation codes require detailed surface loading inputs that can only be supplied by an acoustic code such as described here [15]. The current design philosophy for propeller driven airliners includes aft-mounted engines where propeller tip clearance from the fuselage is small. Both single rotor and contra-rotating propellers are proposed for propulsion. Near-field computation is essential for fuselage structure in the vicinity of the propeller. The present code is highly suitable for this purpose.

ACKNOWLEDGEMENTS

REFERENCES

1. J. H. BRAHNEY 1985, Aerospace Engineering, February issue, 7-10, Is the Unducted Fan Tomorrow's Subsonic Engine?

2. J. E. FFOWCS WILLIAMS 1984, IMA Journal of Applied Mathematics, 32, 113-124, Acoustic Analogy.

3. P. A. NYSTROM and F. FARASSAT 1980, NASA Technical Paper 1662, A Numerical Technique for Calculation of the Noise of High-Speed Propellers with Advanced Blade Geometry.

4. W. E. ZORUMSKI and D. S. WEIR (editors) 1986, NASA Technical Memorandum 83199 Part 3, Aircraft Noise Prediction Program Theoretical Manual—Propeller Aerodynamics and Noise.

5. D. B. HANSON and M. R. FINK 1979, Journal of Sound and Vibration, 62, 19-38, The Importance of Quadrupole Sources in Prediction of Transonic Tip Speed Propeller Noise.

6. K. D. KORKAN, E. VON LAVANTE and T. A. WHITE 1986, AIAA-86-0468, Numerical Evaluation of Propeller Noise in the Near and Far Field.

7. F. FARASSAT 1981, AIAA Journal, 19, 1122-1130, Linear Acoustic Formulas for Calculation of Rotating Blade Noise.

8. F. FARASSAT and G. P. SUCCI 1983, Vertica, 7(4), 309-320, The Prediction of Helicopter Rotor Discrete Frequency Noise.

9. F. FARASSAT 1985, AGARD-CP-366 (10) 1-15, Theoretical Analysis of Linearized Acoustics and Aerodynamics of Advanced Supersonic Propellers.

10. F. FARASSAT 1986, AIAA Journal, 24 (4), 578-584, The Prediction of the Noise of Advanced Propellers in the Time Domain.

11. J. D. DENTON and U. K. SINGH 1979, VKI Lecture Series 1979-7, Time Marching Methods for Turbomachinery Flow Calculation, In Application of Numerical Methods to Flow Calculations in Turbomachiens, Von Karman Institute for Fluid Dynamics.

12. P. M. MORSE 1948, Vibration and Sound, 2nd Edition, New York: McGraw-Hill Book Co.

13. B. M. BROOKS and K. G. MACKALL 1984, AIAA-84-0250, Measurement and Analysis of Acoustic Flight Test Data for Two Advanced Design High Speed Propeller Models.

14. J. ATVARS, L. K. SCHUBERT, E. GRANDE and H. S. RIBNER 1966, NASA Contractor Report 494. Refraction of Sound by Jet Flow or Jet Temperature.

15. L. D. POPE, E. G. WILBY and J. F. WILBY 1984, NASA Contractor Report 3813, Propeller Aircraft Interior Noise.

16. I. M. GEL'FAND and G. E. SHILOV 1964, Generalized Functions (Vol. 1) Properties and Operations. New York: Academic Press.

17. R. P. KANWAL 1983, Generalized Functions – Theory and Technique, New York: Academic Press.

18. F. FARASSAT 1983, AIAA-83-0743, The Prediction of the Noise of Supersonic Propellers in the Time Domain – New Theoretical Results.

APPENDIX

In this appendix a brisk derivation of the theoretical formulations used in developing the code reported here is given. Readers should consult original references for more detailed derivation. Consider the following wave equation:

$$\Box^2 \phi = \frac{\partial}{\partial x_i} [Q_i |\nabla f| \delta(f)] \qquad i = 1\text{-}4 \qquad (A1)$$

where x_i, i=1-3 are the space variables and x_4=ct. The summation convention of tensor analysis is used in this equation. As is obvious from the Dirac delta function $\delta(f)$, the moving source surface is described by f=0. The formal solution of Eq. (A1) is

$$4\pi\phi(\underset{\sim}{x},t) = \frac{\partial}{\partial x_i} \int \frac{1}{r} Q_i |\nabla f| \delta(f)\delta(g) d\underset{\sim}{y} d\tau \qquad (A2)$$

where g=τ-t+r/c, r=$\left|\underset{\sim}{x}-\underset{\sim}{y}\right|$ and $(\underset{\sim}{x},t)$ and $(\underset{\sim}{y},\tau)$ are observer and source space-time variables respectively.

It is a significant fact that the derivatives with respect to observer space variables in Eq. (A2) can be converted to observer time differentiation exactly. One utilizes the following relation

$$\frac{\partial}{\partial x_i} [\frac{\delta(g)}{r}] = -\frac{\partial}{\partial x_4} [\frac{\hat{r}_i \delta(g)}{r}] - \frac{\hat{r}_i \delta(g)}{r^2} \qquad i = 1\text{-}3 \qquad (A3)$$

where $\hat{r}_i=(x_i-y_i)/r$, i=1-3, is the unit vector in radiation direction. Using Eq. (A3) in Eq. (A2) results in

$$4\pi\phi(\underset{\sim}{x},t) = \frac{\partial}{\partial x_4} \int \frac{1}{r} (Q_4 - Q_r) \left| \nabla f \right| \delta(f)\delta(g)d\underset{\sim}{y}d\tau$$

$$- \int \frac{Q_r}{r^2} \left| \nabla f \right| \delta(f)\delta(g)d\underset{\sim}{y}d\tau \tag{A4}$$

where $Q_r = Q_i \hat{r}_i$, $i=1-3$. The interpretation of integrals involving products of delta functions are given elsewhere [7, 16, 17]. Let the surface Σ be described by $F(\underset{\sim}{y}; \underset{\sim}{x},t) = [f(\underset{\sim}{y},\tau)]_{ret} = 0$, then Eq. (A4) can be written as

$$4\pi\phi(\underset{\sim}{x},t) = \frac{\partial}{\partial x_4} \int_{F=0} \frac{1}{r} \left[\frac{Q_4 - Q_r}{\Lambda}\right]_{ret} d\Sigma - \int \frac{1}{r^2} \left[\frac{Q_r}{\Lambda}\right]_{ret} d\Sigma \tag{A5}$$

where

$$\Lambda^2 = 1 + M_n^2 - 2M_n \cos\theta \tag{A6}$$

In Eq. (1), $Q = (-p\underset{\sim}{n}, M_n)$ so that the solution of Eq. (1), using Eq. (A5) is

$$4\pi p'(\underset{\sim}{x},t) = \frac{1}{c}\frac{\partial}{\partial t} \int_{F=0} \frac{1}{r} \left[\frac{M_n + p\cos\theta}{\Lambda}\right]_{ret} d\Sigma + \int_{F=0} \frac{1}{r^2} \left[\frac{p\cos\theta}{\Lambda}\right]_{ret} d\Sigma \tag{A7}$$

This equation, referred to as Formulation 1, was coded in a high speed propeller noise prediction program by Nystrom and Farassat [3] for both subsonic and supersonic sources. It is used in the ANOPP program [4] for supersonic sources only. It was also coded for helicopter rotor noise prediction. The following relation was used to write Eq. (A7) in two equivalent forms for subsonic and supersonic sources [7]

$$\frac{d\Sigma}{\Lambda} = \frac{dS}{\left|1 - M_r\right|} = \frac{cd\tau d\Gamma}{\sin\theta} \tag{A8}$$

where $d\Gamma$ is element of the curve of intersection of the surfaces $f=0$ and $g=0$.

Because of excessive execution time on a computer and sensitivity to errors of numerical differentiation of Eq. (A7), two different results were derived for subsonic and supersonic sources. For subsonic case, using the integration on the actual blade surface (from Eq. A8)), the time derivative of Eq. (A7) was taken inside the first integral, resulting in Eq. (2) of this paper [8].

For supersonic sources, a singularity-free formulation is much more difficult to derive. In Eq. (1), $\underset{\sim}{Q}$ is decomposed into two vector fields $\underset{\sim}{Q}_N$ and $\underset{\sim}{Q}_T$ normal and tangent to the surface f=0 in <u>four dimensions</u>. Here $\underset{\sim}{Q}_N$ and $\underset{\sim}{Q}_T$ are [9, 10]

$$\underset{\sim}{Q}_N = - \frac{1}{\alpha_n^2} (p + M_n^2)(\underset{\sim}{n}, -M_n) \tag{A9a}$$

$$\underset{\sim}{Q}_T = \frac{1}{\alpha_n^2} M_n(1 - p) (\underset{\sim}{M}_n, 1) \tag{A9b}$$

Equation (1) then can be written, for an open piece of the surface as

$$\Box^2 p = \nabla_4 \cdot [H(k) \underset{\sim}{Q}_N |\nabla f| \delta(f)] + \nabla_4 \cdot [H(k) \underset{\sim}{Q}_T |\nabla f|] \delta(f) \tag{A10}$$

where k=0 together with f=0 define the edge of the open surface.

The interpretation of the second term of Eq. (A10) is easy. The first term requires a great deal of algebra. Using Green's function of the wave equation, an integral of the following kind is obtained

$$I = \int \frac{\delta'(g)}{r} \nabla_4 \cdot [H(k) \underset{\sim}{Q}_N |\nabla f|] \delta(f) \ dy d\tau + \int \frac{1}{r^2} \cdots dy d\tau \tag{A11}$$

where the second integral is of a conventional type involving $\delta(f)\delta(g)$ which results in a surface integral on surface Σ. Using an identity of generalized

functions [18], the first integral can be written as the sum of two integrals involving $\delta(f)\delta(g)$ and $\delta(f)\delta(g)\delta(k)$, respectively. The integral whose integrand has $\delta(f)\delta(g)\delta(k)$ gives the line integrals in Eqs. (3) and (4). The complexity of these equations have come from the attempt to write each term of the final integrands in explicit forms for computer coding. It should be noted a relation similar to Eq. (A8) exists for line sources which was utilized in coding [18]:

$$\frac{d\gamma}{\Lambda_o} = \frac{dl}{\left|1-M_r\right|} = \frac{cd\tau}{\left|\cos\psi\right|} \tag{A12}$$

Here dl is the element of length of the edge of the open surface and ψ is the local angle that the edge makes with radiation direction $\hat{\underset{\sim}{r}}$.

Nomenclature

$\tilde{B}^i$ $i=1,2$ components of $\underset{\sim}{b}$ along the direction of the principal curvatures. Basis vectors assumed unit length.

$\underset{\sim}{b}$ $= \lambda \underset{\sim}{M}_t + \lambda_1 \underset{\sim}{t}_1; \; b = \left| \underset{\sim}{b} \right|$

b_ν $\underset{\sim}{b} \cdot \underset{\sim}{\nu}$

c speed of sound

$F(\underset{\sim}{y};\underset{\sim}{x},t)$ $=f(\underset{\sim}{y},t-r/c) = [f(\underset{\sim}{y},\tau)]_{ret}$

$F_m(\underset{\sim}{y};\underset{\sim}{x},t)$ $= f_m(\underset{\sim}{y},t-r/c) = [f_m(\underset{\sim}{y},\tau)]_{ret}$

$f(\underset{\sim}{y},\tau)=0; \; f(\underset{\sim}{x},t)=0$ The equation of the blade surface in the frame fixed to the undisturbed medium

$f_m(\underset{\sim}{y},\tau)=0, \; f_m(\underset{\sim}{x},t)=0$ The equation of the mean blade surface in the frame fixed to the undisturbed medium

g $= \tau - t + r/c$

$H(k)$ Heaviside function

H The local mean curvature of the blade surface

h_n $= \lambda M_n + \lambda_1 \cos\theta$

$K(\underset{\sim}{y};\underset{\sim}{x},t)=0$ $= [k(\underset{\sim}{y},\tau)]_{ret}$

$k=0$ The equation of a surface whose intersection with $f=0$ produces a finite open piece of the blade surface by relations $f=0$, $k>0$.

1 (in dl) length variable along the trailing edge, along perimeter of airfoil section, at blade inner radius or along shock traces

$\underset{\sim}{M}$ Local Mach number vector based on c, $M_n = \underset{\sim}{M} \cdot \underset{\sim}{n}$, $M_r = \underset{\sim}{M} \cdot \hat{\underset{\sim}{r}}$

$\underset{\sim}{M}_p$ The projection of the Mach number vector on the local plane normal to the edges (e.g., TE) of blade surface, $M_p = \left| \underset{\sim}{M}_p \right|$

$\underset{\sim}{M}_t$ The projection of M on the local tangent plane of the blade surface for fixed source time τ, $\dot{M}_t = \left| \underset{\sim}{M}_t \right|$

$\underset{\sim}{N}$ The four-dimensional unit vector normal to $f(\underset{\sim}{y},\tau) = 0$ described by $(\underset{\sim}{n}, -M_n)/\alpha_n$

$\underset{\sim}{n}, n_1$ Unit normal to $f=0$, τ-fixed

p' Acoustic pressure (nondimensional)

$P_B(\underset{\sim}{n},\tau)$ $\equiv p(\underset{\sim}{y}(\underset{\sim}{n},\tau),\tau)$ blade surface pressure described in a frame moving with the blades (nondimensional)

Q'_N $= \lambda[2\lambda_1(\cos\theta - M_n)+1]$

Q_F $= \frac{1}{c}(2\lambda^2 - \frac{1}{\tilde{\Lambda}^2})\dot{M}_n + \frac{1}{c}\underset{\sim}{\Omega}\cdot[\frac{\underset{\sim}{M}_t \underset{\sim}{-t}_1}{\tilde{\Lambda}^2} - 2\lambda\underset{\sim}{b} + (\frac{1}{\tilde{\Lambda}^2} + 2\lambda\lambda_1)\underset{\sim}{r}] + 2b^2\kappa_b + \kappa_1\sigma_{11} + \kappa_2\sigma_{22} - 2Hh_n$

Q'_F $= \frac{\lambda}{c}\dot{P}_B - b\frac{\partial P_B}{\partial\sigma_b} + 2M_n[\frac{1}{c}(\lambda\dot{M}_n - \underset{\sim}{\Omega}\cdot\underset{\sim}{b}) + \kappa_1\tilde{\mu}^1\tilde{B}^1 + \kappa_2\tilde{\mu}^2\tilde{B}^2]$

Q''_F $= \frac{1}{c}(\dot{M}_n - \underset{\sim}{\Omega}\cdot\underset{\sim}{M}_t) + \kappa_M M_t^2 - 2HM_n^2$

$\bar{Q}''_F$ $= \frac{1}{c}(\dot{M}_n - \underset{\sim}{\Omega}\cdot\underset{\sim}{M}_t) + \bar{\kappa}_M M_t^2$; $\bar{\kappa}_M$ is the average of the normal curvatures of the upper and lower blade surfaces in the direction of $\underset{\sim}{M}_t$.

Q_E $= \lambda M_{a\nu} + \lambda_1\hat{r}_\nu$, $M_{a\nu} = \underset{\sim}{M}\cdot\underset{\sim}{\nu}$, $\underset{\sim}{M}$ based on absolute velocity

$\underset{\sim}{r}, r_1$ $= \underset{\sim}{x} - \underset{\sim}{y}$, $r = |\underset{\sim}{x} - \underset{\sim}{y}|$

$\hat{\underset{\sim}{r}}, \hat{r}_1$ Unit radiation vector $\underset{\sim}{r}/r$

$\hat{r}_\nu$ $\hat{\underset{\sim}{r}}\cdot\underset{\sim}{\nu}$

$\hat{\underset{\sim}{r}}_p$ Unit vector in the direction of the projection of $\hat{\underset{\sim}{r}}$ on the local plane normal to the edges (e.g., TE) of blade surface, τ-fixed

S (in dS) element of blade surface area

t Observer time

$\underset{\sim}{t}_1$ The projection of the unit radiation vector $\hat{\underset{\sim}{r}}$ on the local tangent plane to $f=0$, τ-fixed. Not unit vector, $|\underset{\sim}{t}_1| = \sin\theta$

Greek Symbols

α_n $= (1 + M_n^2)^{1/2}$

γ (in dγ) length variable along the intersection of an edge of $f=0$ (e.g., TE) and the collapsing sphere $g=0$

Γ (in dΓ) length variable of the arc of intersection of surfaces $f=0$ and $g=0$

∇_4	The 4-D gradient (∇_y, $1/c \, \partial/\partial\tau$), $\nabla_y = \partial/\partial y_i$
$\delta(f)$	The Dirac delta function
θ	The angle between $\underset{\sim}{n}$ and $\hat{\underset{\sim}{r}}$
$\underset{\sim}{n}$	The Lagrangian coordinate of a point on the surface $f=0$
Λ	$= (1 + M_n{}^2 - 2M_n\cos\theta)^{1/2}$
$\tilde{\Lambda}$	$= (\Lambda^2 + \sin^2\theta)^{1/2}$
Λ_0	$= [M_p{}^2\cos^2\psi + (1 - \underset{\sim}{M}_p \cdot \hat{\underset{\sim}{r}}_p \sin\psi)^2]^{1/2}$
$\tilde{\mu}^i$	$i = 1,2$ components of $\underset{\sim}{M}_t$ in the direction of principal curvatures. Basis vectors assumed unit length.
$\underset{\sim}{\nu}, \nu_i$	unit inward geodesic normal, i.e. The surface vector perpendicular to an edge (e.g., TE) of the surface $f=0$, τ-fixed
ρ_0	density of undisturbed medium
$\sim$	(in $d\Sigma$) surface area of $F=0$
σ_b	the length parameter on $f=0$ along $\underset{\sim}{b}$
σ_{11}, σ_{22}	two components of tensor $(\underset{\sim}{t}_1\underset{\sim}{t}_1 - \underset{\sim}{M}_t\underset{\sim}{M}_t + \underset{\sim}{t}_1\underset{\sim}{M}_t + \underset{\sim}{M}_t\underset{\sim}{t}_1)/\tilde{\Lambda}^2$,
ψ	the local angle between r and an edge of $f=0$
$\underset{\sim}{\Omega}, \Omega_i$	$= \underset{\sim}{n} \times \underset{\sim}{\omega}$
κ_1, κ_2	principal curvatures of the surface $f=0$
$\kappa_M, \kappa_t, \kappa_b$	normal curvatures along $\underset{\sim}{M}_t$, $\underset{\sim}{t}_1$, and $\underset{\sim}{b}$, respectively
λ	$= (\cos\theta - M_n)/\tilde{\Lambda}^2$
λ_1	$= (\cos\theta + M_n)/\tilde{\Lambda}^2$
$\underset{\sim}{\omega}$	angular velocity

Other symbols are defined in the text.

Table 1.- Blade data and operating conditions

Design	SR-3
No. of blades	8
Radius (m)	0.317
RPM	7569
Blade angle, 3/4 radius (degrees)	58.9
Advance ratio	3.030
Tip helical Mach number	1.134
Forward speed (m/sec)	242.3
Horsepower	223.7
Power coefficient	1.828

Table 2.- Boom microphone positions

Microphone No.	Radial Distance (m)	Axial Distance (m)
1	0.824	0.305
3	0.824	−0.008
4	0.824	−0.252

Convention for axial distance: positive ahead of the disk
negative behind the disk

Table 3.— Grid system used in study of converence and computation time

Grid System	Coarse Grid	Fine Grid	Relative Computation Time
1	A	5×5	0.27
2	A	10×10	0.33
3	B	10×10	1.00
4	C	10×10	3.47

Table 4.— The acoustic pressure spectra at boom microphone 4 for grid systems of Table 3. Boom reflection correction is not included. ε=0.05.

HARMONIC		GRID SYSTEM 1			GRID SYSTEM 2		
NUMBER	FREQUENCY (Hz)	THICKNESS NOISE (dB)	LOADING NOISE (dB)	OVERALL NOISE (dB)	THICKNESS NOISE (dB)	LOADING NOISE (dB)	OVERALL NOISE (dB)
1	1009.20	147.43	139.75	147.06	140.64	138.76	140.39
2	2018.39	133.76	134.90	132.57	135.41	134.13	135.15
3	3027.59	129.06	130.09	128.77	131.77	128.83	129.87
4	4036.78	127.35	126.58	130.84	127.59	125.53	126.15
5	5045.98	132.90	123.22	130.54	129.90	122.95	128.65
6	6055.17	127.45	120.77	126.32	127.42	120.17	125.12
7	7064.37	131.93	121.52	130.49	128.14	120.85	126.99
8	8073.56	124.67	110.38	124.19	124.54	111.81	123.94
9	9082.76	123.96	117.08	119.75	124.21	115.95	120.28
10	10091.95	121.55	115.93	123.62	122.82	115.78	124.08
..	11101.15	122.24	109.98	123.39	120.54	106.02	119.26
12	12110.34	125.27	110.34	123.63	117.83	110.84	115.60
13	13119.54	119.31	109.44	121.82	116.14	105.90	114.77
14	14128.73	120.55	111.17	117.29	116.34	108.70	115.02
15	15137.93	118.51	91.59	118.32	114.91	87.51	114.55
			OASPL	147.80		OASPL	142.64

HARMONIC		GRID SYSTEM 3			GRID SYSTEM 4		
NUMBER	FREQUENCY (Hz)	THICKNESS NOISE (dB)	LOADING NOISE (dB)	OVERALL NOISE (dB)	THICKNESS NOISE (dB)	LOADING NOISE (dB)	OVERALL NOISE (dB)
1	1009.20	138.15	139.04	138.81	137.85	139.03	138.70
2	2018.39	135.90	133.97	136.20	135.73	133.93	135.92
3	3027.59	132.00	128.46	130.63	132.10	128.55	130.95
4	4036.78	129.49	125.16	127.60	129.79	125.19	127.58
5	5045.98	128.41	123.01	126.82	128.38	122.94	126.86
6	6055.17	127.94	120.75	127.22	127.74	120.69	127.02
7	7064.37	126.18	118.11	124.66	126.24	118.04	124.68
8	8073.56	124.32	116.03	121.95	124.30	116.07	122.23
9	9082.76	122.40	114.67	120.75	122.42	114.55	120.83
10	10091.95	120.63	113.14	119.81	120.98	113.05	120.30
11	11101.15	120.34	110.89	119.17	120.87	110.73	120.13
12	12110.34	118.26	108.33	116.43	119.47	108.41	118.36
13	13119.54	115.88	107.12	114.75	116.47	107.30	115.64
14	14128.73	115.01	104.53	114.57	115.88	106.23	115.60
15	15137.93	114.83	103.19	114.31	115.66	103.85	114.88
			OASPL	141.93		OASPL	141.86

TABLE 4

Table 5.— Acoustic pressure spectra at boom microphone 4 for ε=0.1 and
ε=0.2. Compare with results of Table 4, grid system 3. Grid
system 3 is used in these calculations. Boom reflection
correction is not included.

HARMONIC		GRID SYSTEM 3, ε = 0.1			GRID SYSTEM 3, ε = 0.2		
NUMBER	FREQUENCY (Hz)	THICKNESS NOISE (dB)	LOADING NOISE (dB)	OVERALL NOISE (dB)	THICKNESS NOISE (dB)	LOADING NOISE (dB)	OVERALL NOISE (dB)
1	1009.20	137.86	139.03	138.57	137.90	139.06	138.51
2	2018.39	136.42	133.88	136.57	135.88	134.06	136.10
3	3027.59	131.79	128.44	130.29	132.02	128.61	130.78
4	4036.78	129.56	125.16	127.59	129.64	125.27	127.54
5	5045.98	128.86	122.93	127.21	128.80	123.13	127.37
6	6055.17	127.67	120.88	127.00	127.97	120.91	127.12
7	7064.37	126.56	118.03	125.04	126.49	118.32	124.93
8	8073.56	124.46	116.15	122.06	124.68	116.26	122.71
9	9082.76	122.65	114.65	121.25	122.46	114.69	120.93
10	10091.95	121.02	113.12	120.30	121.00	113.29	120.39
11	11101.15	120.25	111.17	119.54	120.56	111.02	119.53
12	12110.34	119.89	108.33	118.52	118.65	108.89	117.11
13	13119.54	115.01	106.98	113.06	115.98	106.82	115.19
14	14128.73	115.08	104.99	115.34	115.19	105.01	114.81
15	15137.93	115.35	101.28	114.38	115.31	102.69	114.75
			OASPL	141.93		OASPL	141.81

TABLE 5
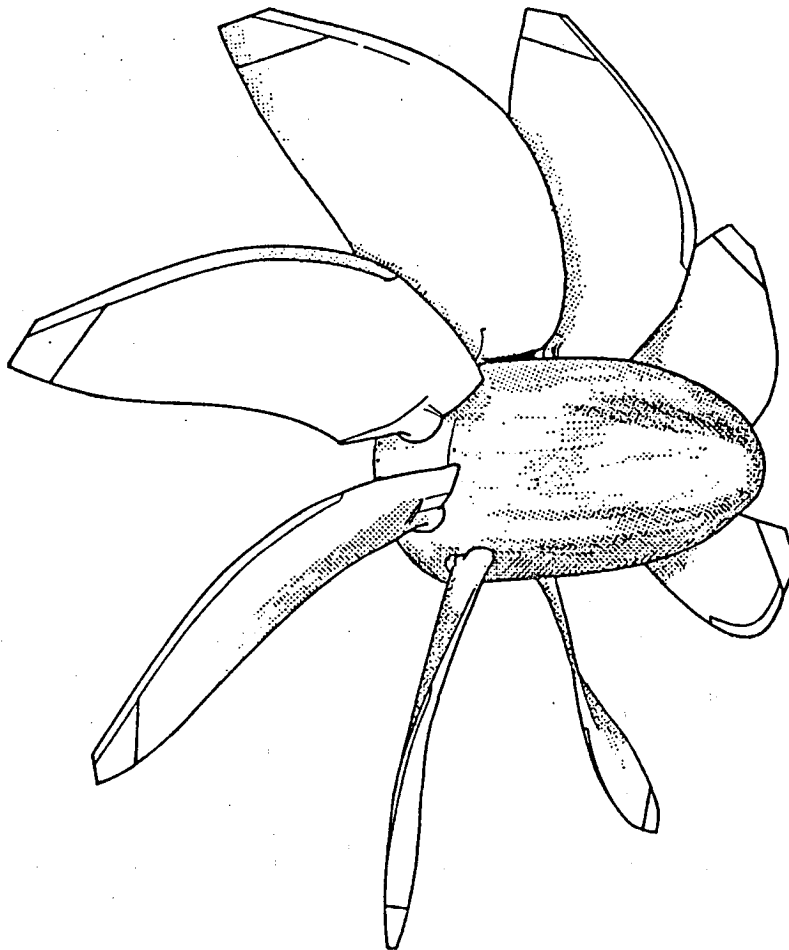
a.

Figure 1.- Examples of (a) single rotor and (b) contra-rotating advanced propellers.
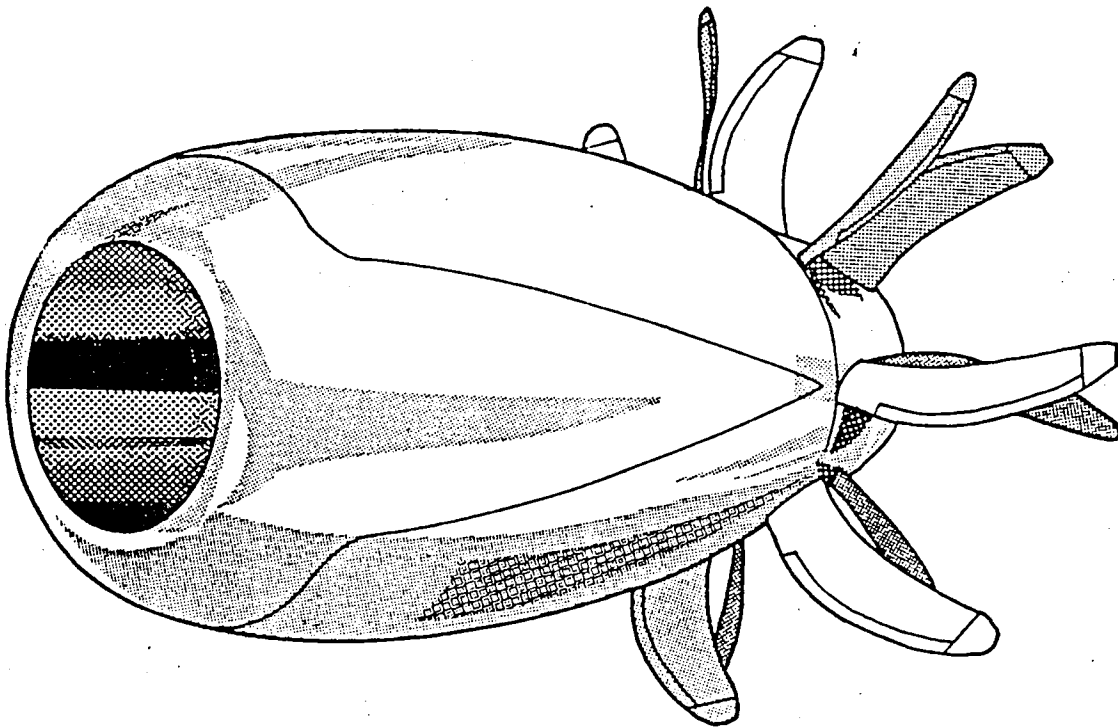
Figure 1b.
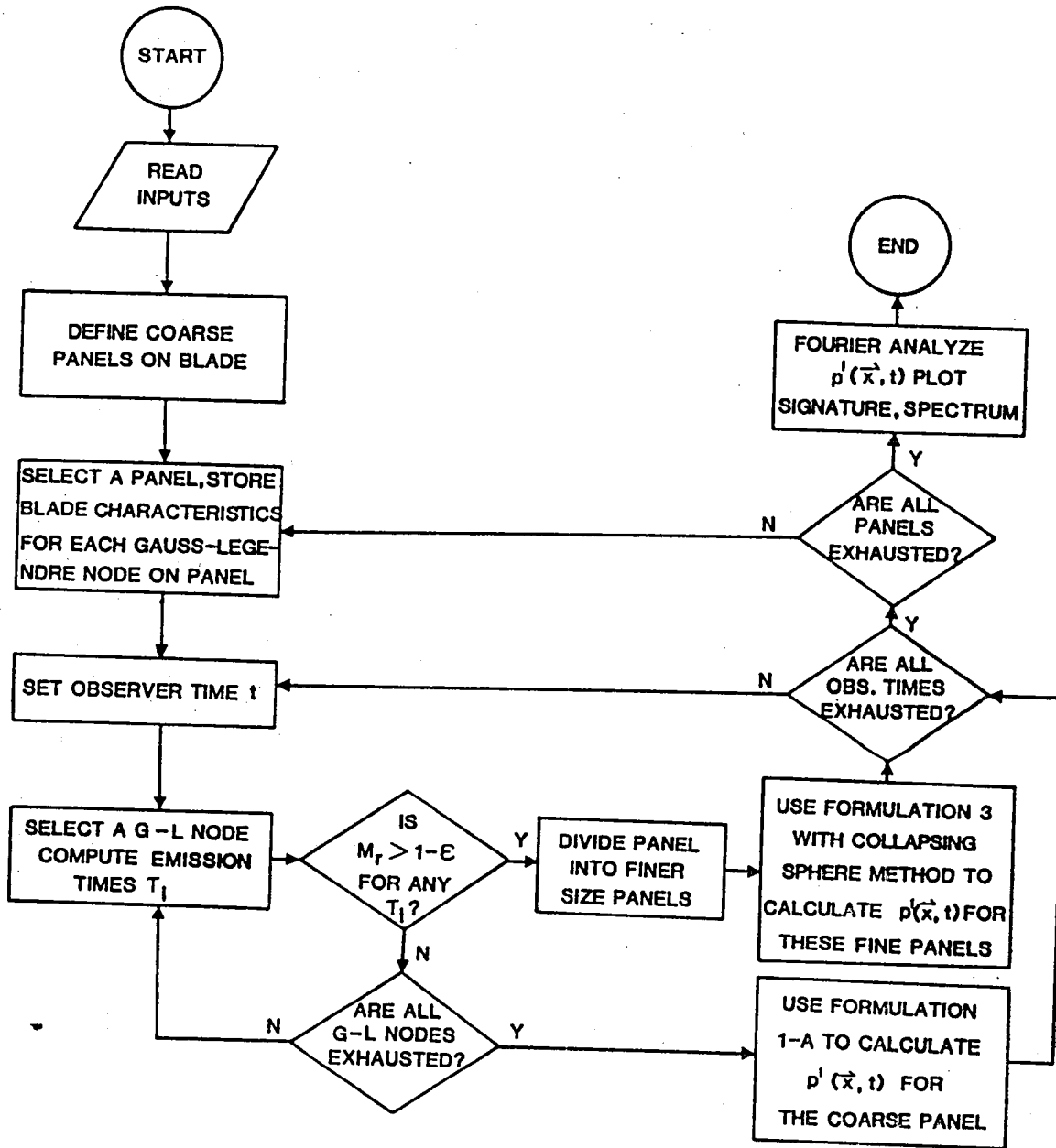
Figure 2.- Flow chart of the computer code.
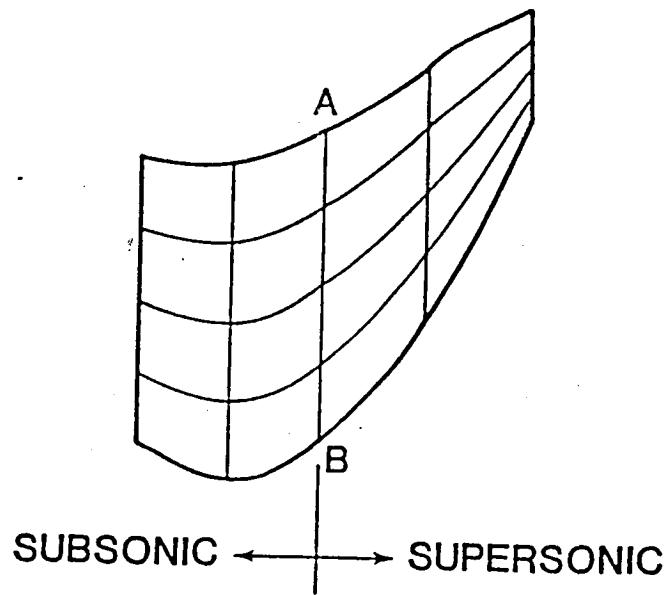
(a) PLANFORM
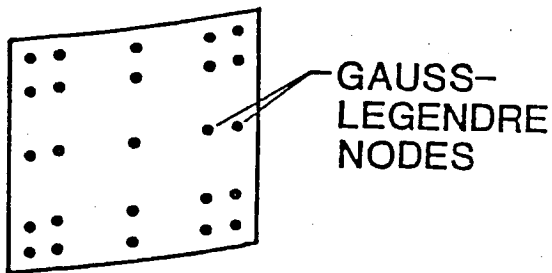
(b) COARSE PANEL-
(FORMULATION 1-A)
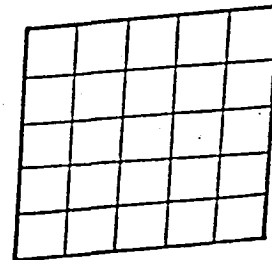
(c) COARSE AND FINE PANELS-
(FORMULATION 3)

Figure 3.- Coarse and fine panels used in the two formulations.
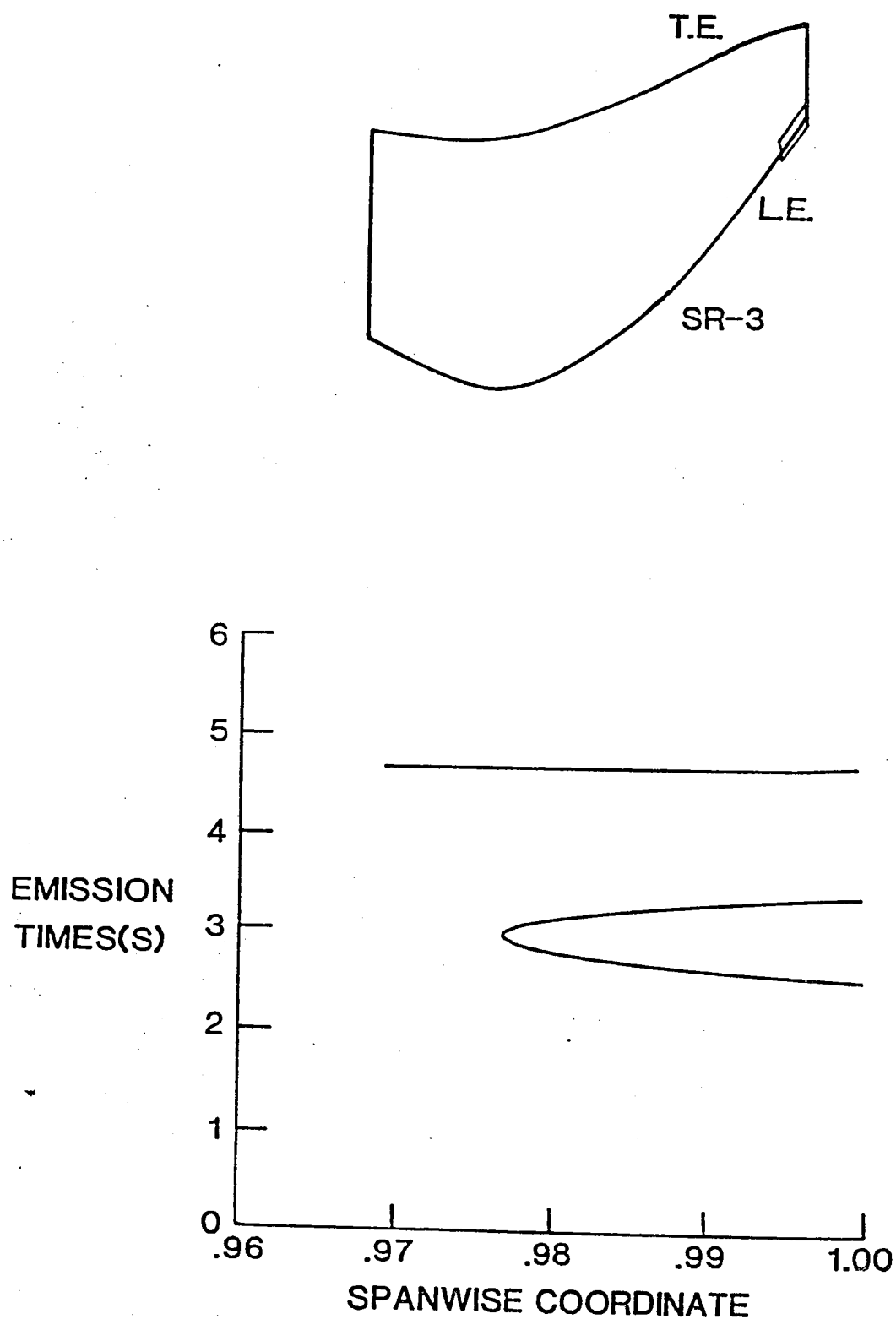
Figure 4.— A test of the emission time calculation routine. The emission time of points on a segment of leading edge at the tip (for a fixed observer time) is plotted versus radial distance. The straight part of the curve has a very small slope and is not constant. Conditions corresponding to microphone 4.
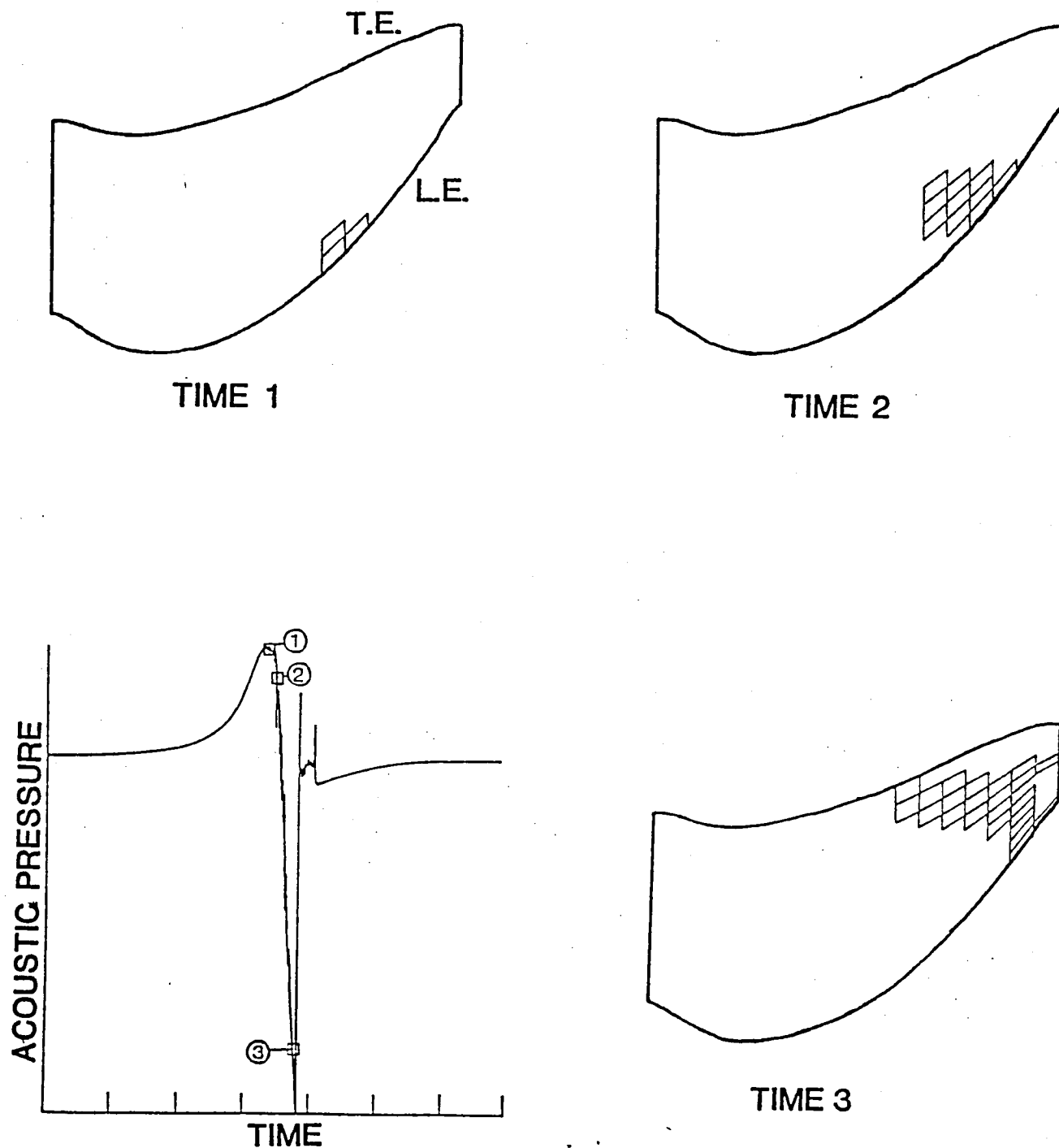
Figure 5.- Panels using Formulation 3 corresponding to three observer time marked on acoustic pressure signature. Single blade.
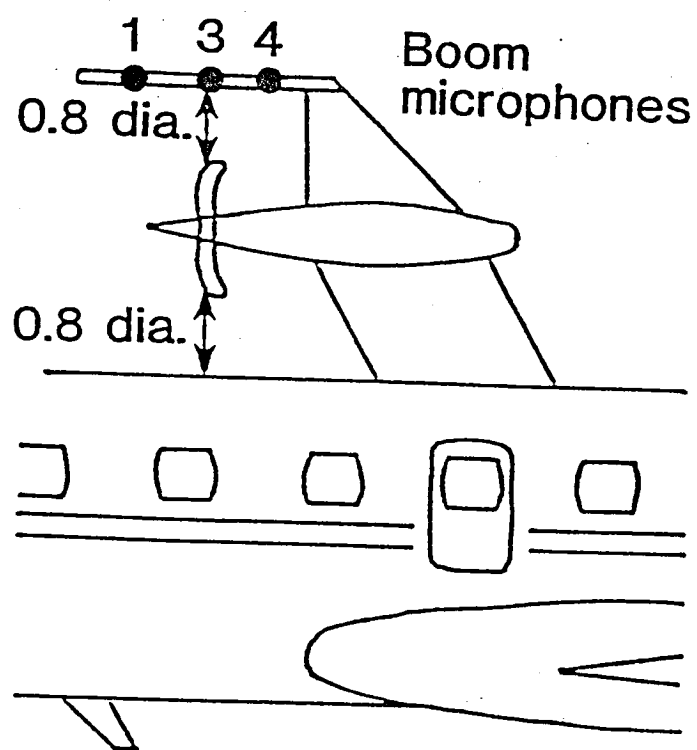
Figure 6.– The test set-up and boom microphones.
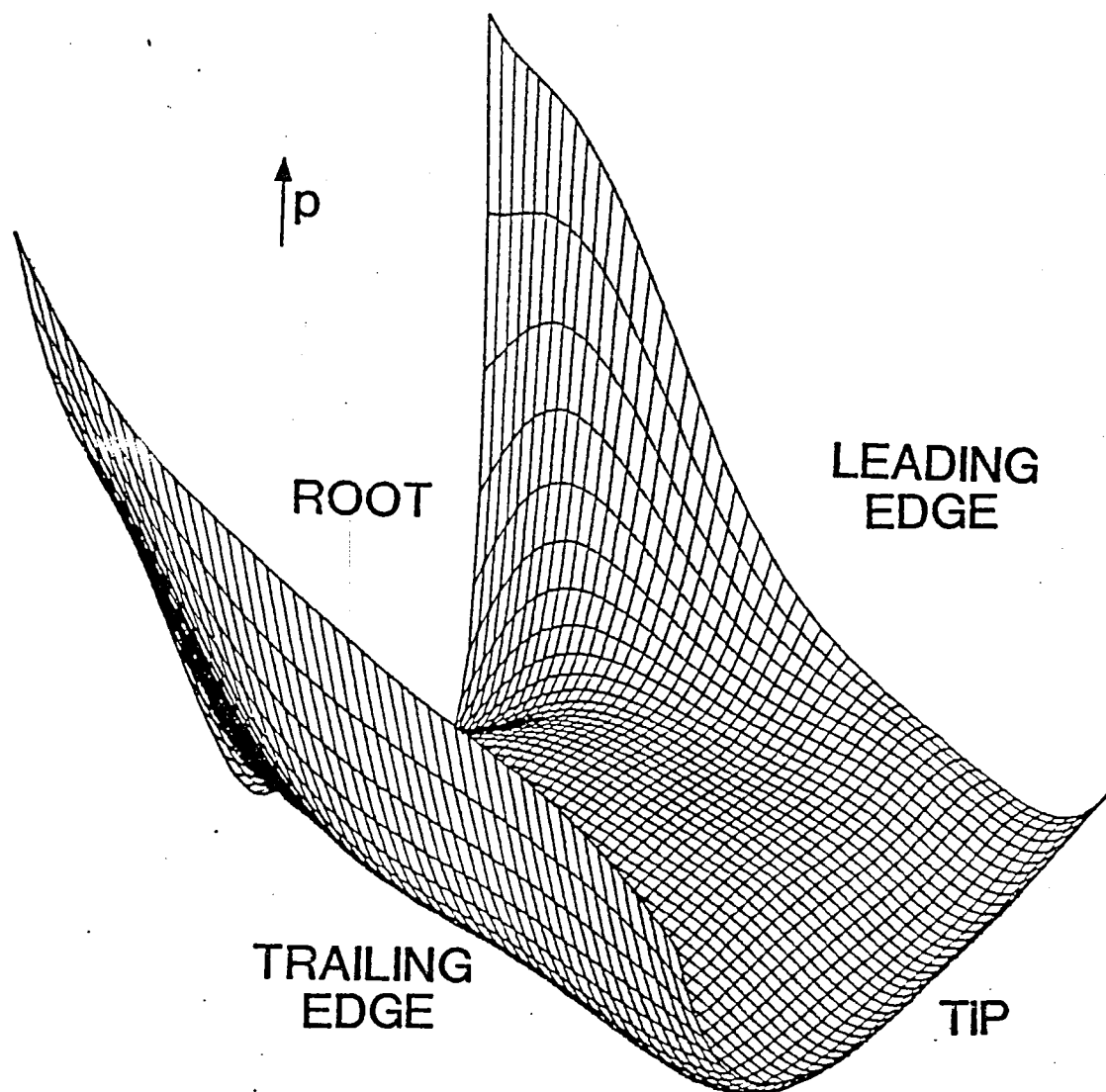
a. UPPER SURFACE

Figure 7.- Blade surface pressure. (a) and (b) 3-D relief, (c) and (d) constant pressure contours, Pa.

b. LOWER SURFACE

Figure 7b.

TIP

CONTOUR FROM   -6000.0   TO   13000. Pa
CONTOUR INTERVAL IS   1000.0

ROOT

c. UPPER SURFACE

Figure 7c.

TIP

H
5781

LEADING EDGE

TRAILING EDGE

1000

4000

1000

1000

1000

1000

8000

1000

12000

0.000

0.000

1000

8000

8000

CONTOUR FROM   -5000.0   TO   23000. Pa
CONTOUR INTERVAL IS   1000.0

ROOT
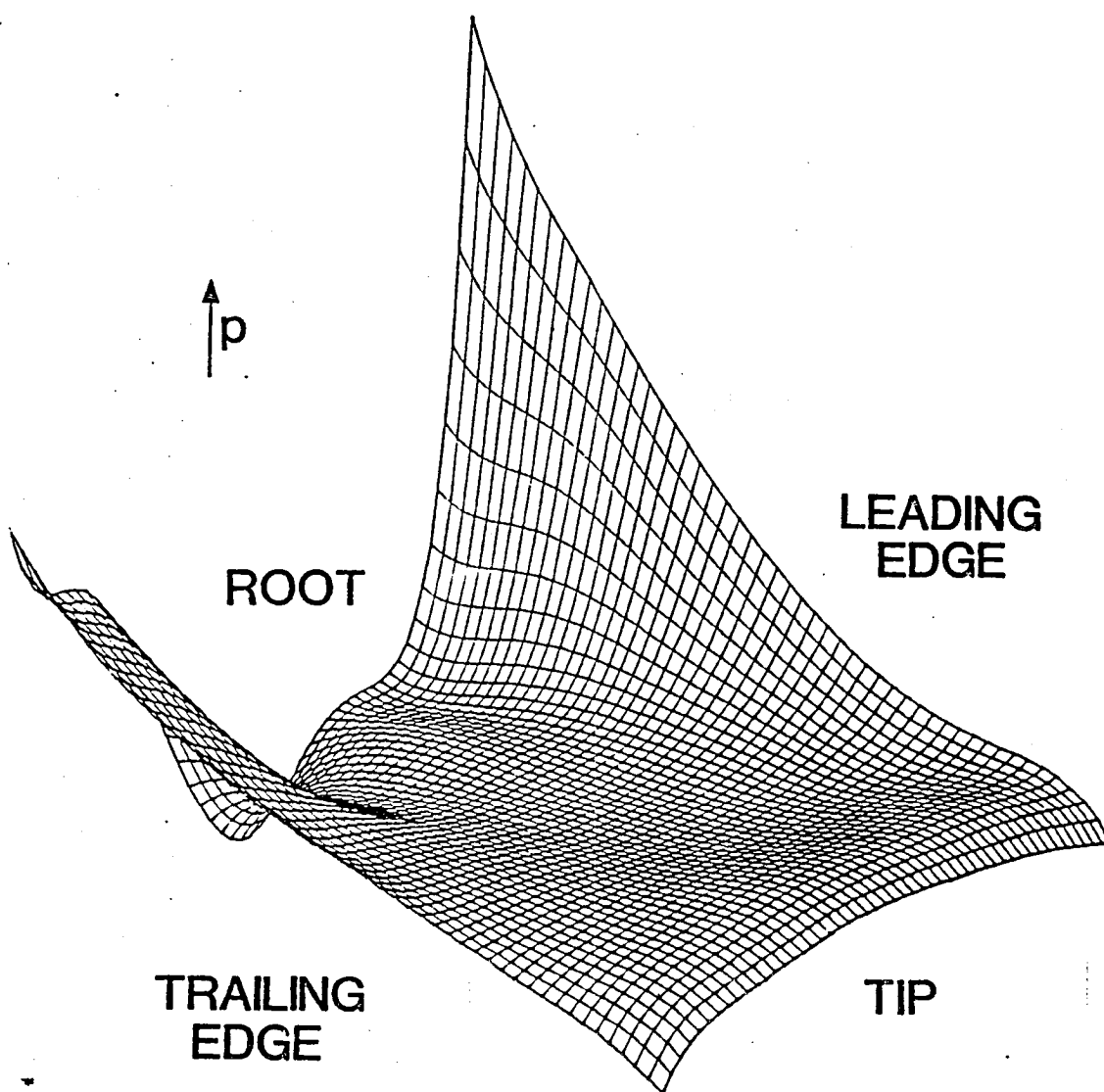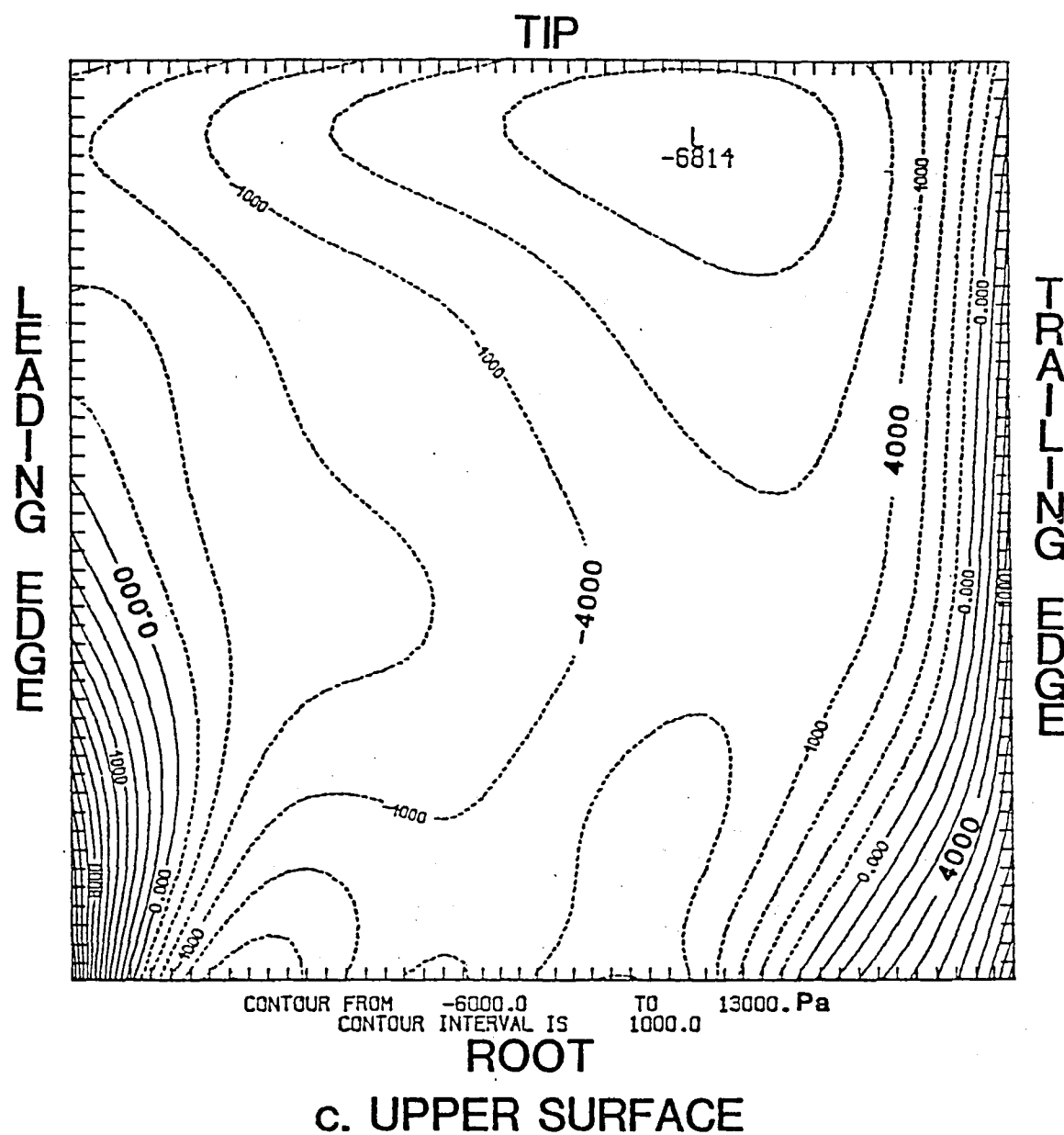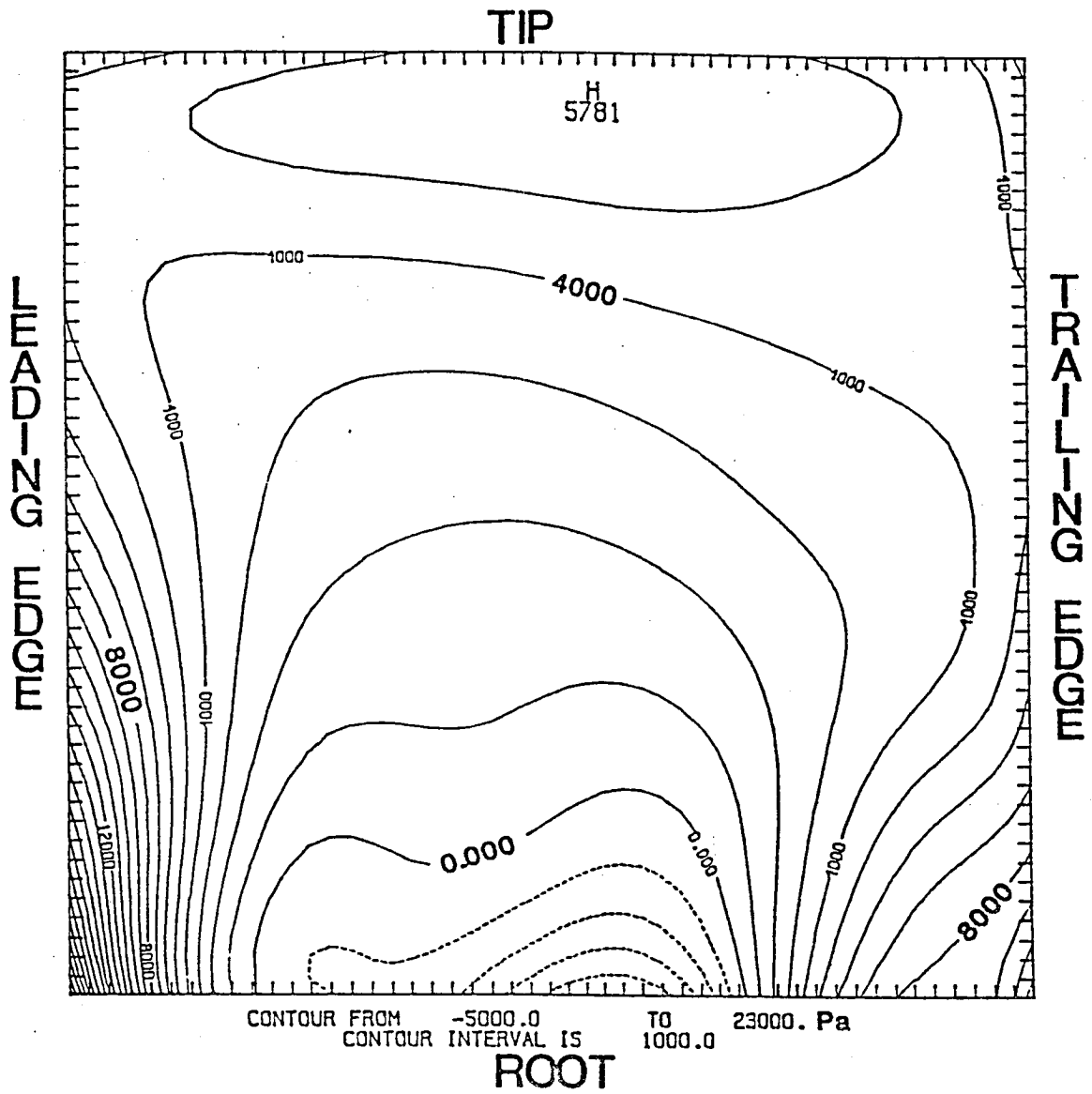
d. LOWER SURFACE
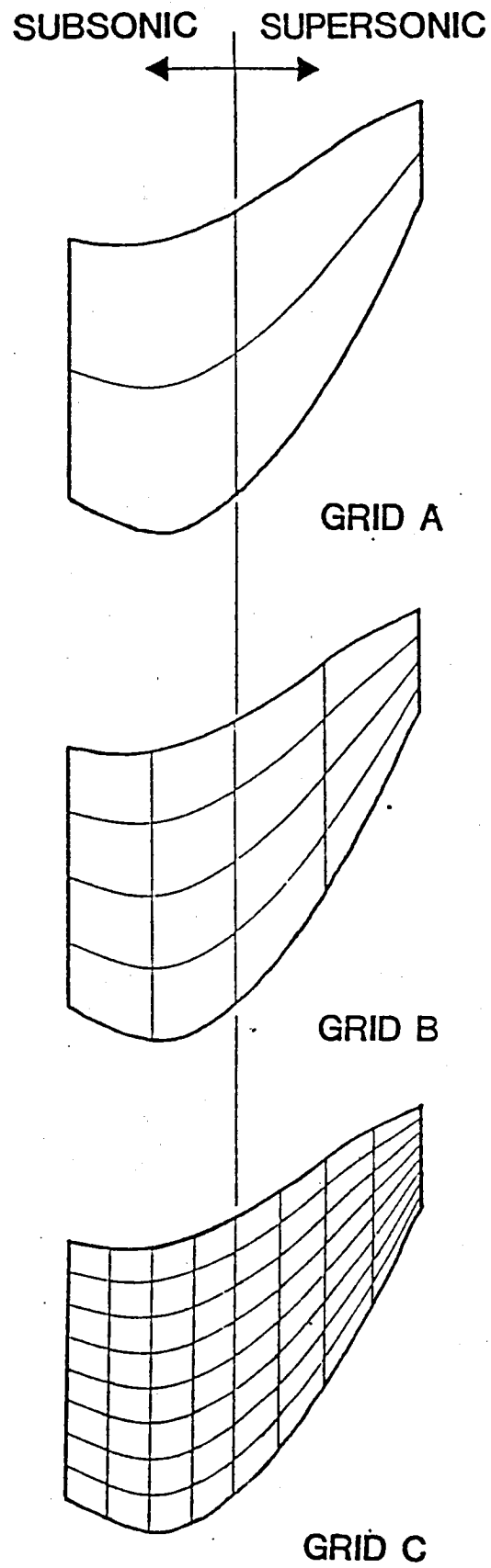
Figure 7d.

Figure 8.- Grids used in grid size study.
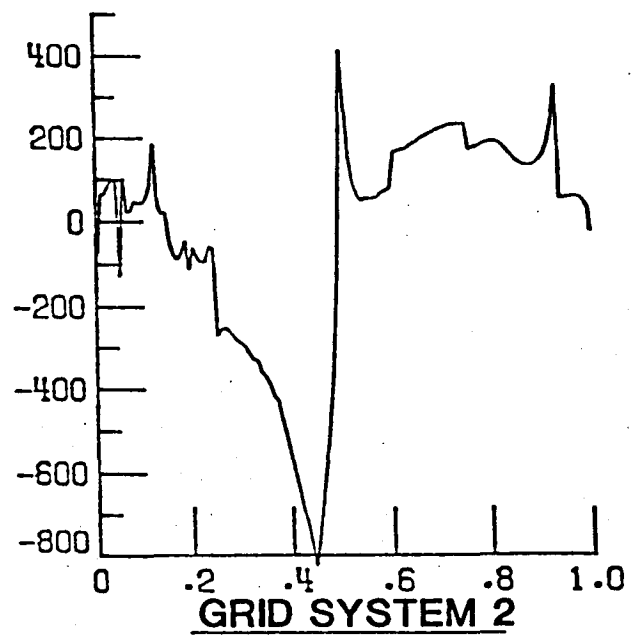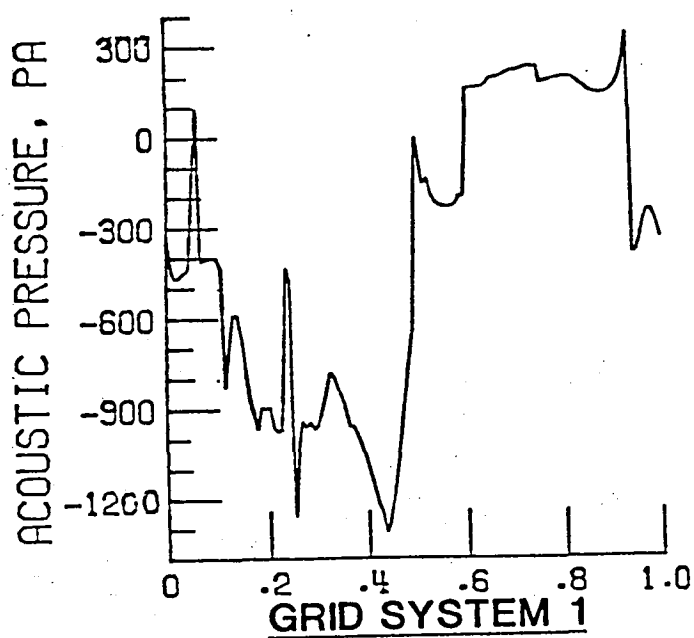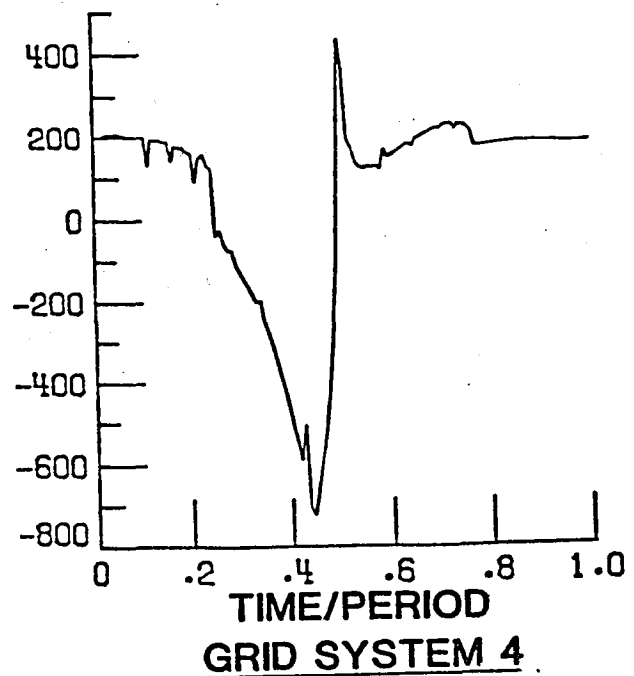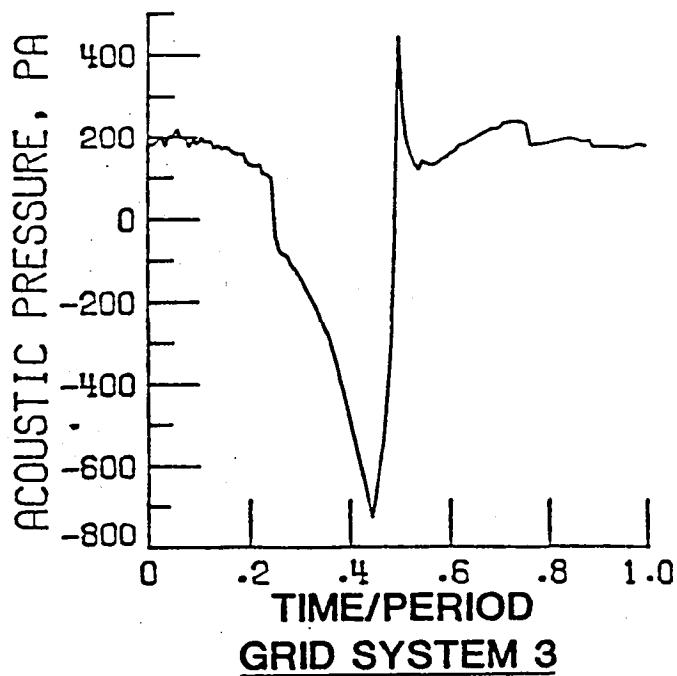
Figure 9.- Acoustic pressure signatures corresponding to grid systems 1-4. Microphone 4, ε=0.05.
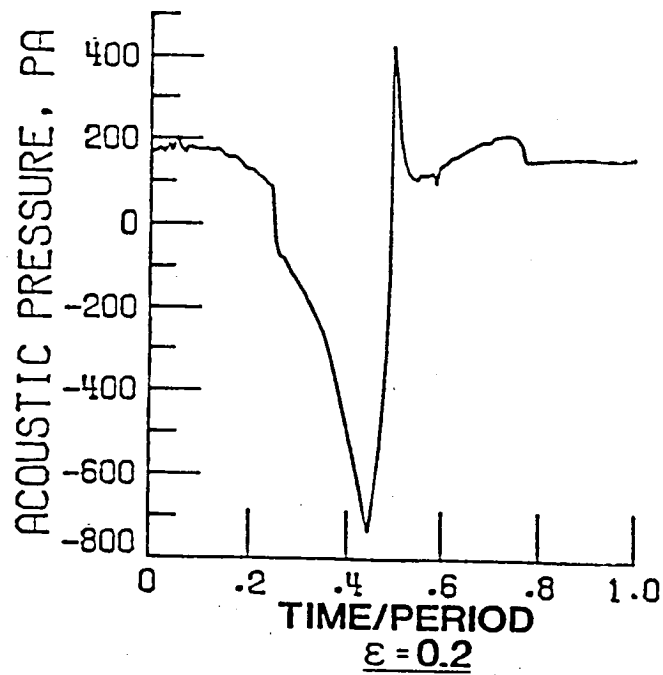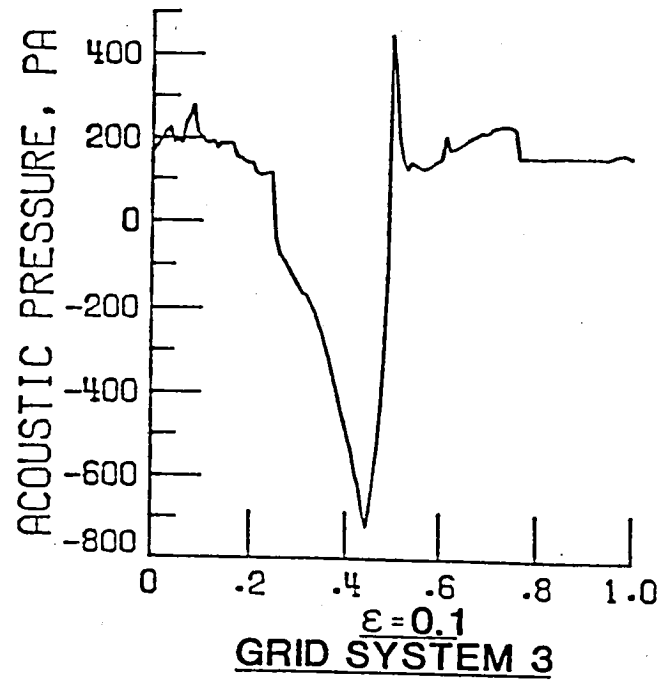
Figure 10.- Acoustic pressure signatures corresponding to ε=0.1 and 0.2.
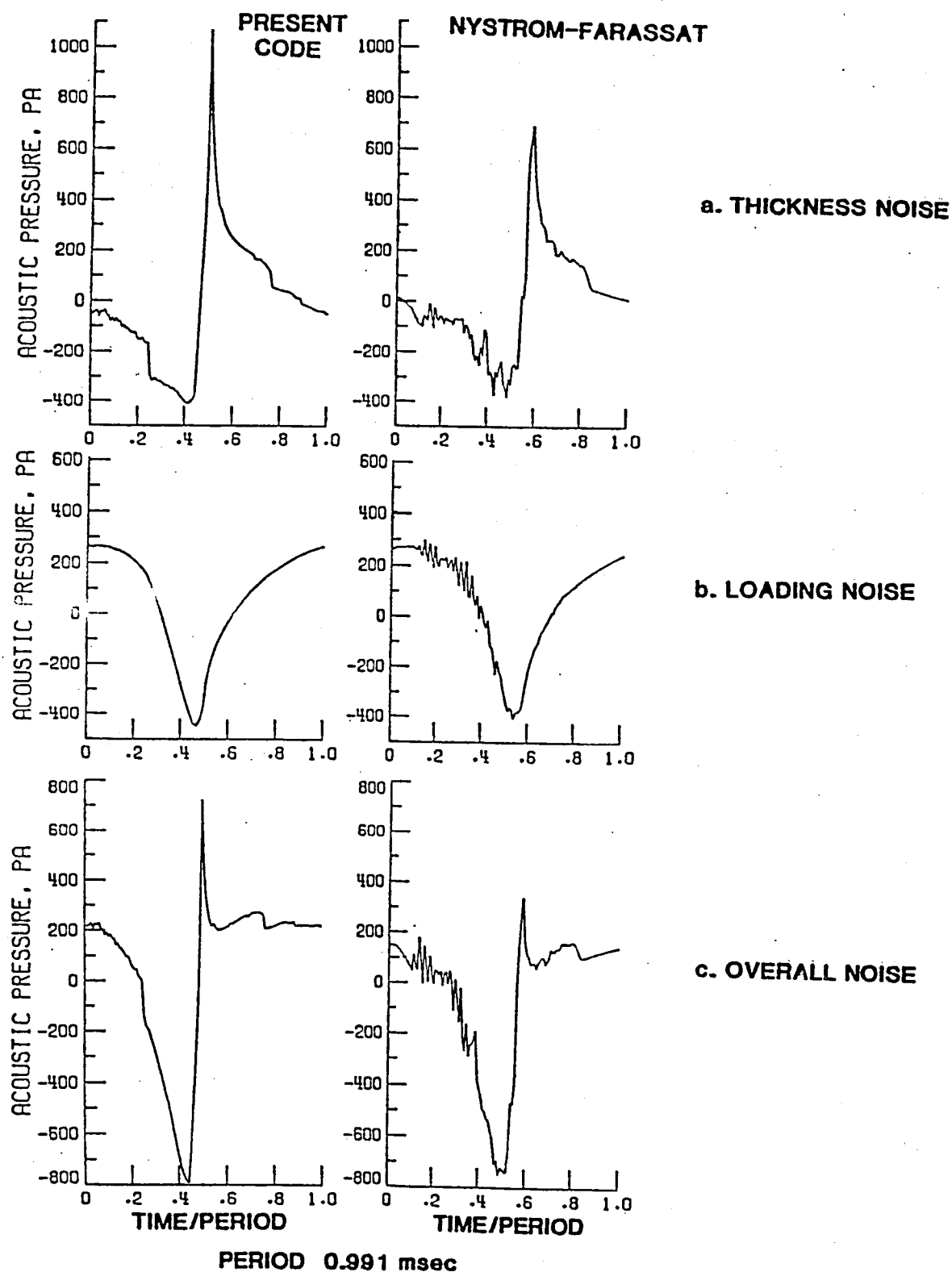
Figure 11.— Comparison of outputs of the present code with Nystrom-Farassat code. (a) thickness noise, (b) loading noise, (c) overall noise.

a- THICKNESS NOISE

b- LOADING NOISE
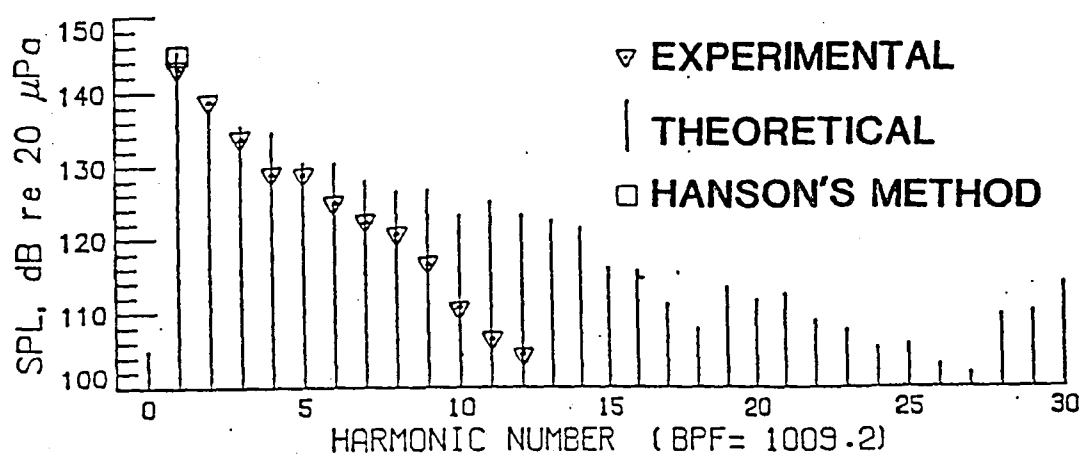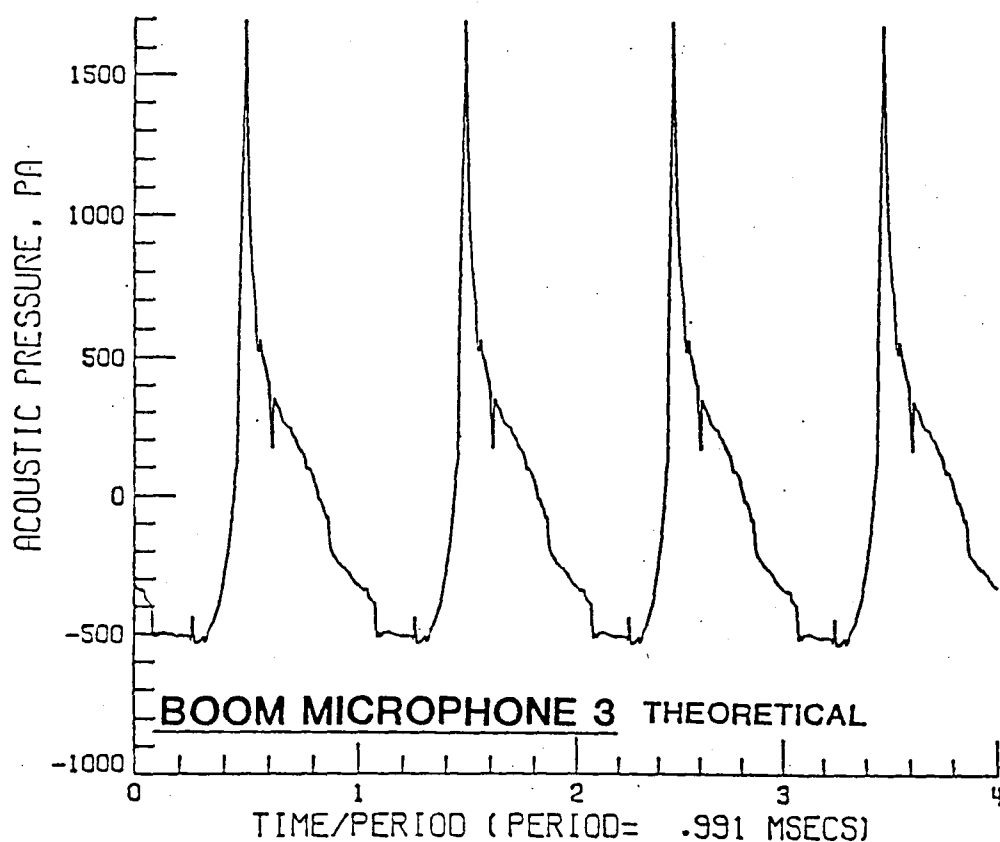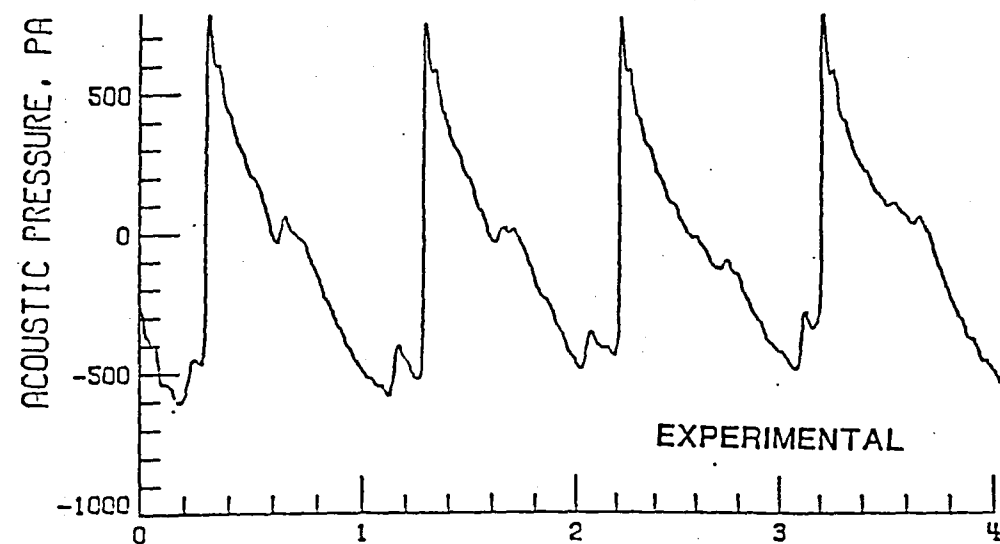
c- OVERALL NOISE
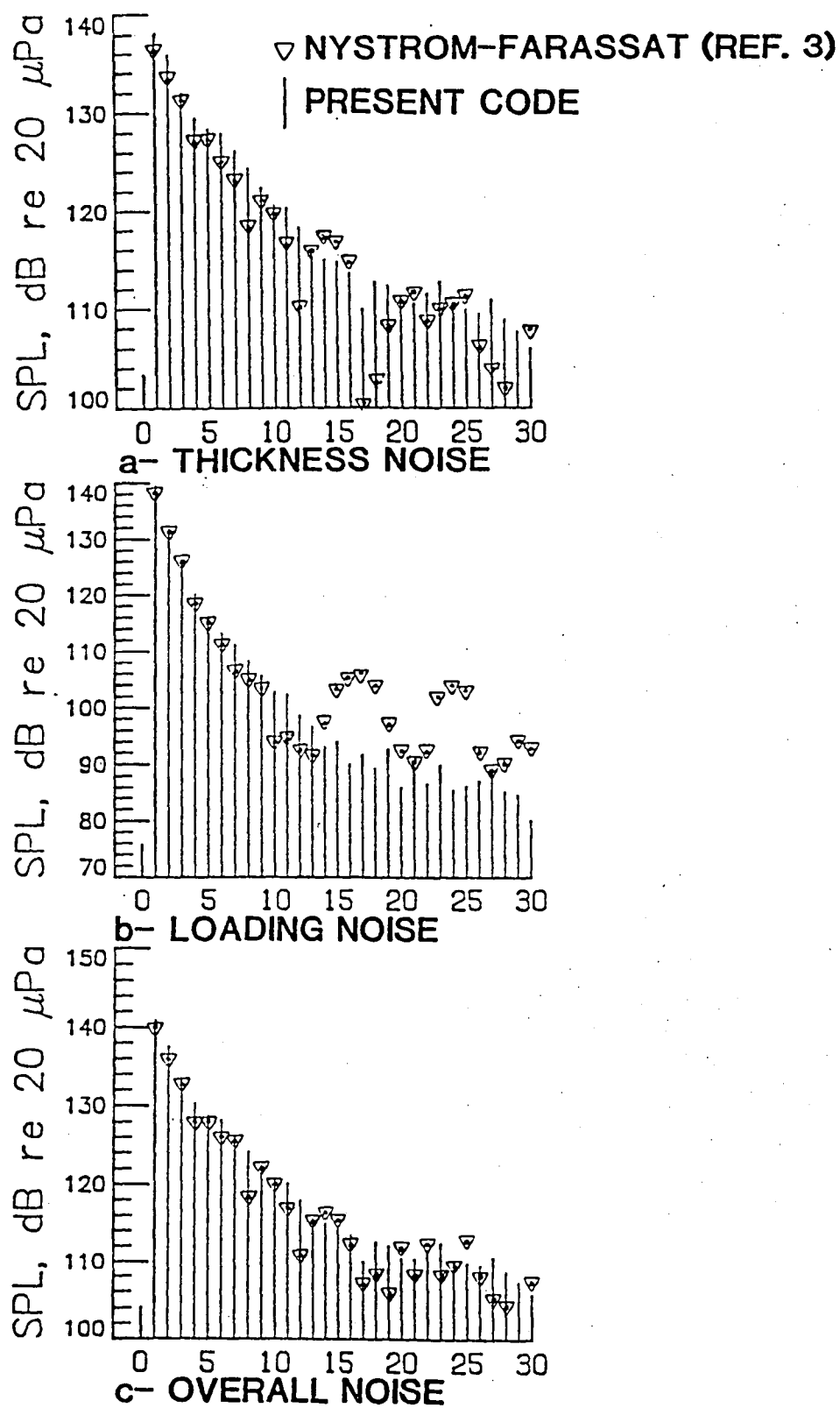
Figure 11 (cont'd).
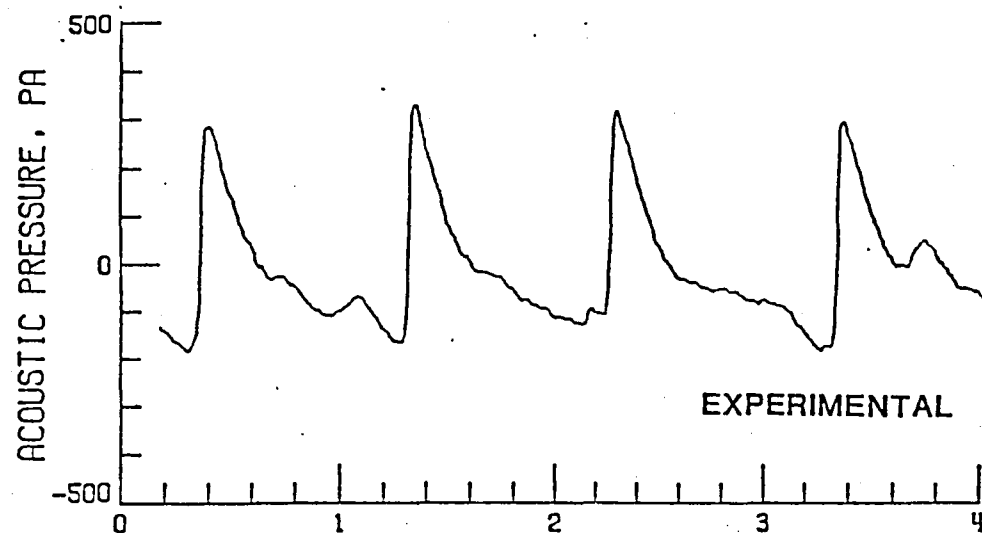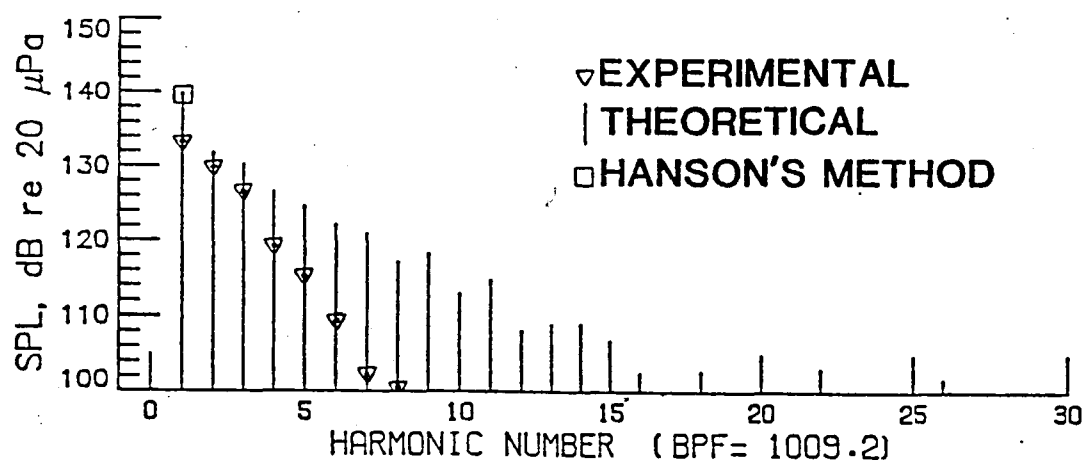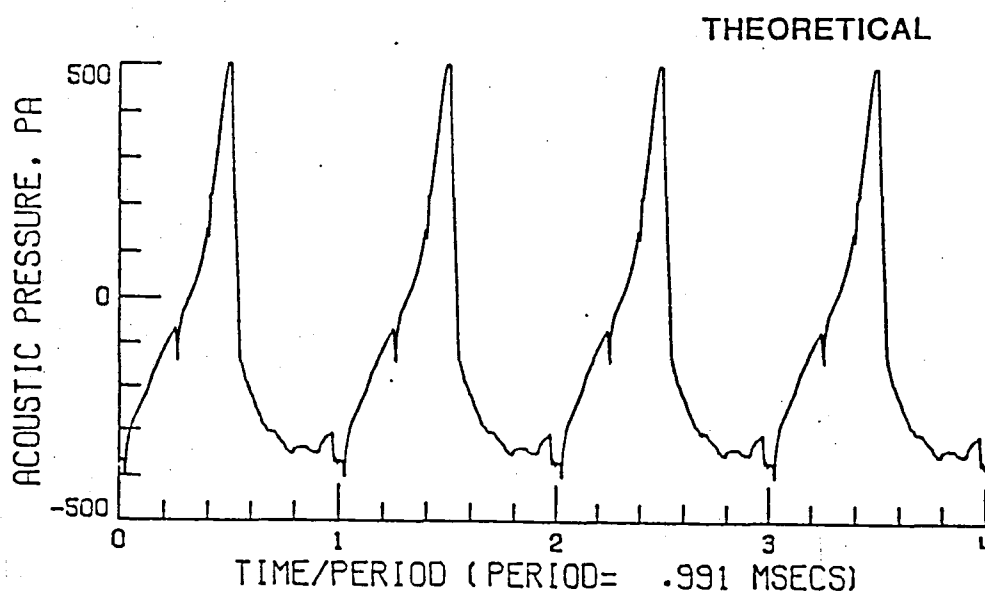
Figure 12.- Comparison of the measured and predicted acoustic pressure
signatures and spectra of microphone 1. Theoretical prediction
corrected for boom reflection.

PROPELLER
DISK

TANGENT
PLANE

IMAGE
PROPELLER
DISK
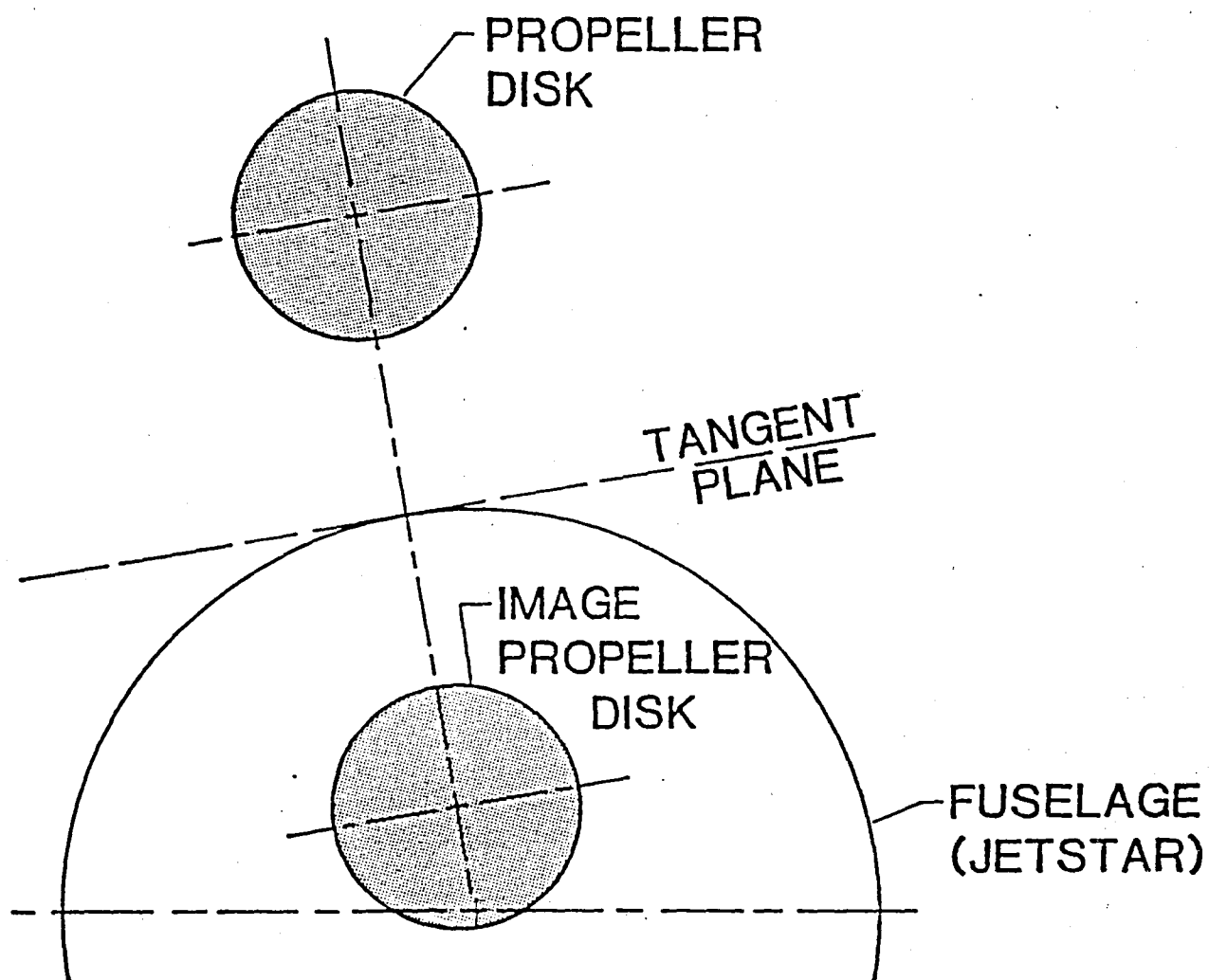
FUSELAGE
(JETSTAR)

Figure 13.- The propeller disk and its image used for fuselage reflection
study.

**BOOM MICROPHONE 1
IMAGE PROPELLER**
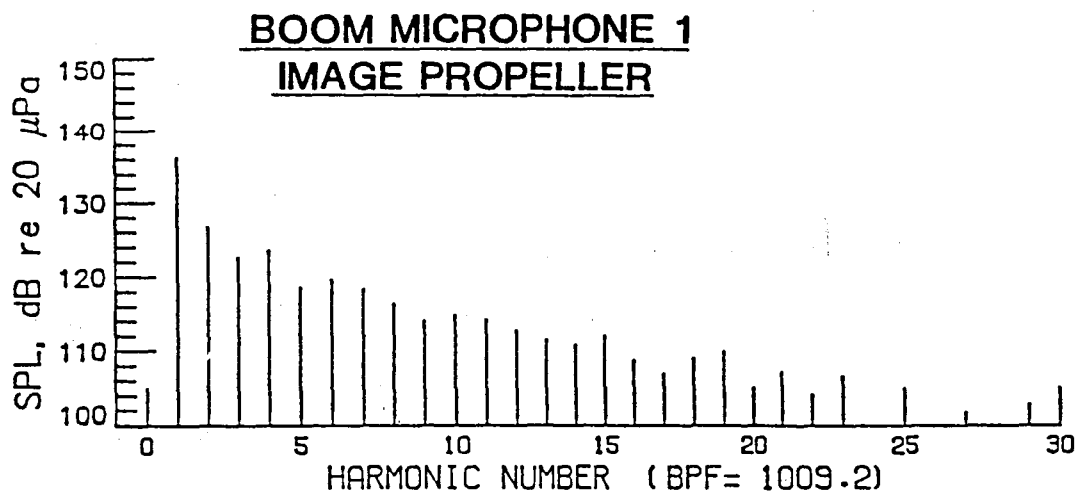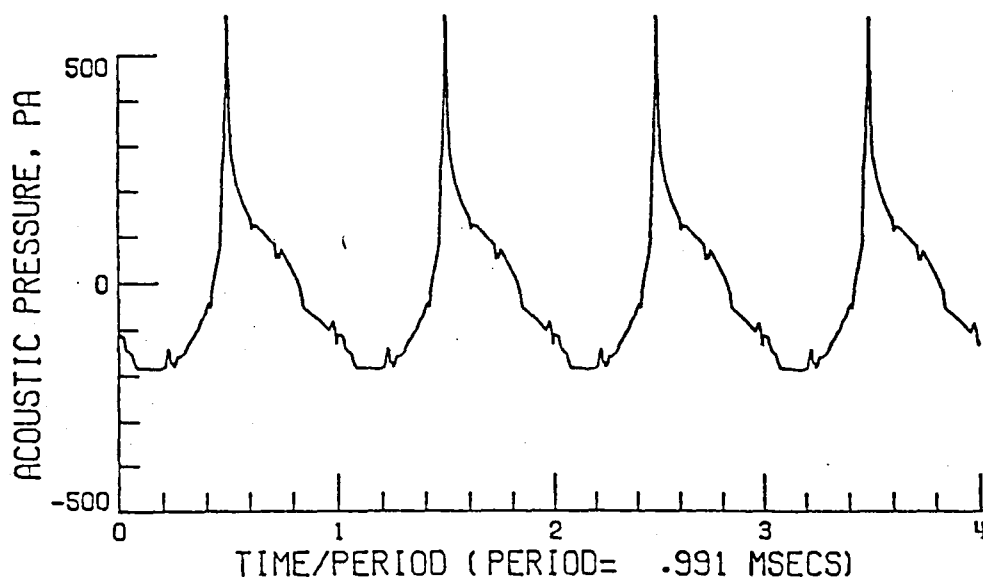
Figure 14.- The acoustic pressure signature and spectrum of image propeller at microphone 1 corrected for boom reflection.
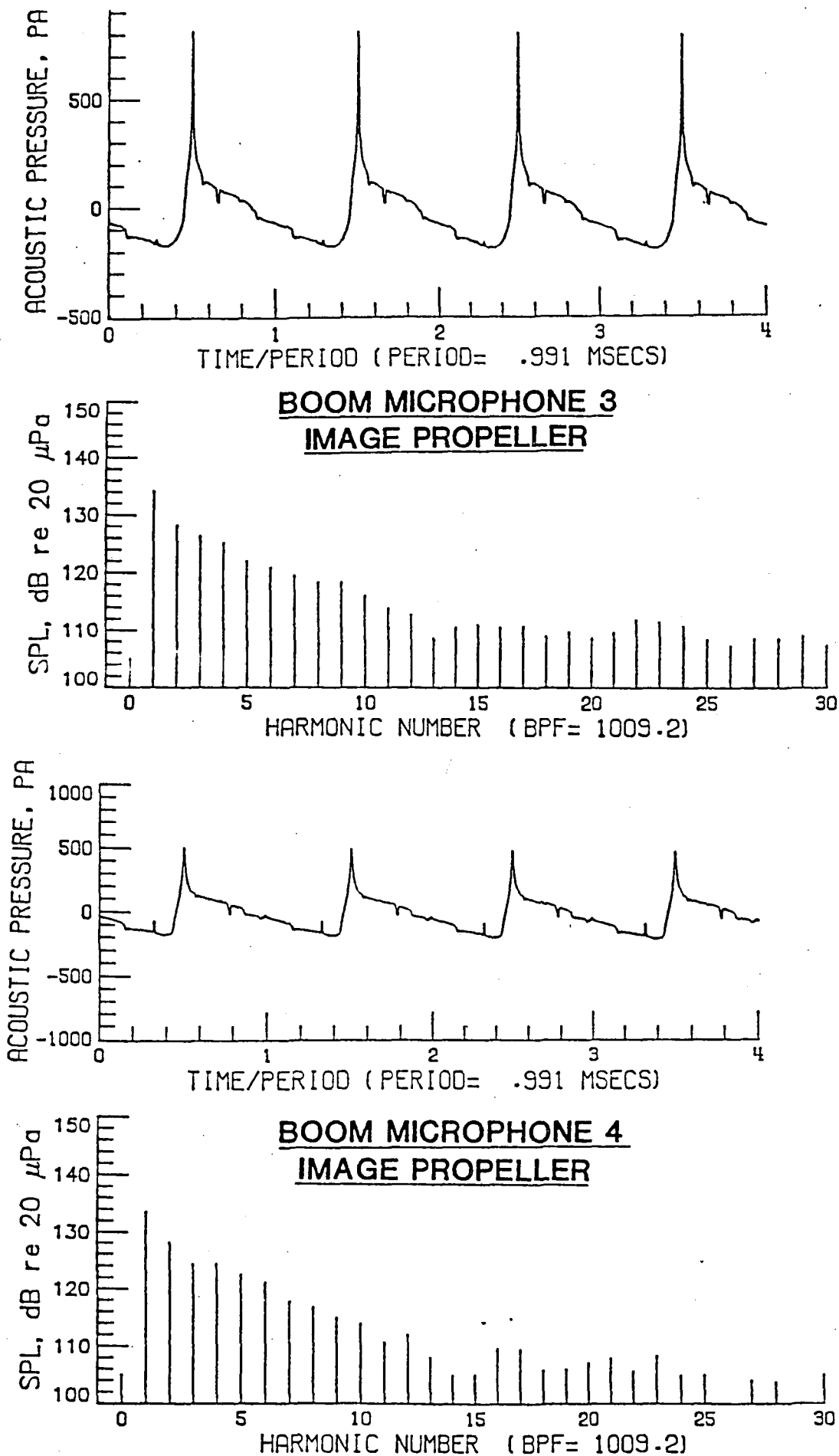
Figure 15.- The acoustic pressure signatures and spectra of image propeller at microphones 3 and 4. Corrected for boom reflection.
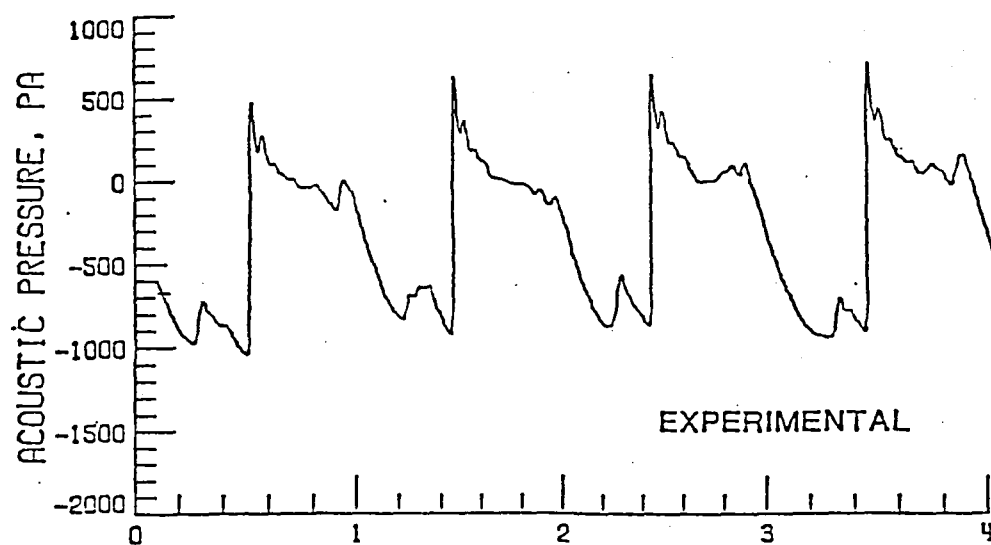
Figure 16.- Comparison of measured and predicted acoustic pressure signatures and spectra at microphone 3. Theoretical prediction corrected for boom reflection.
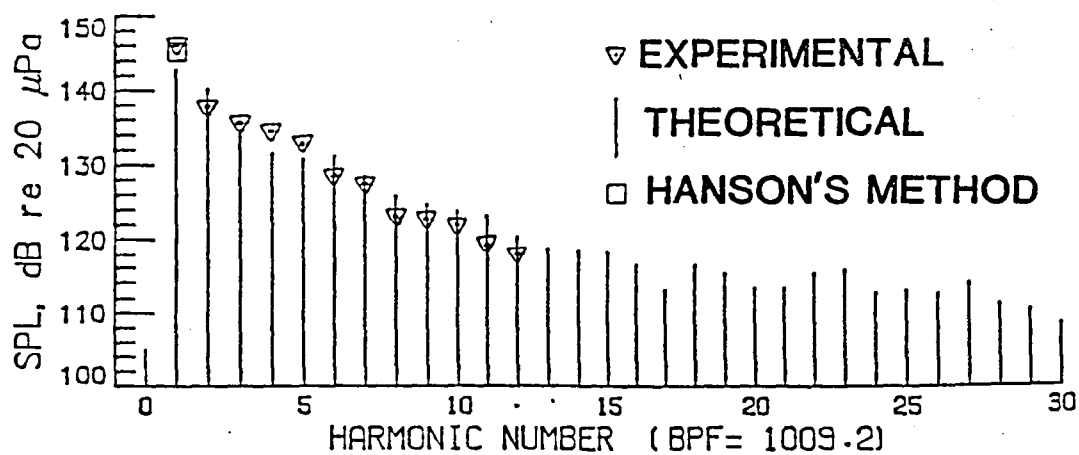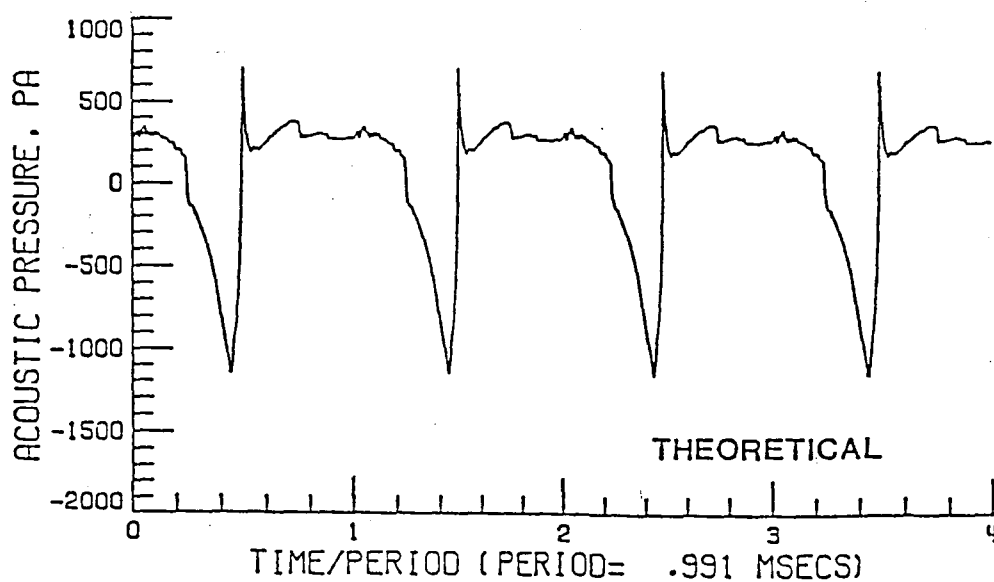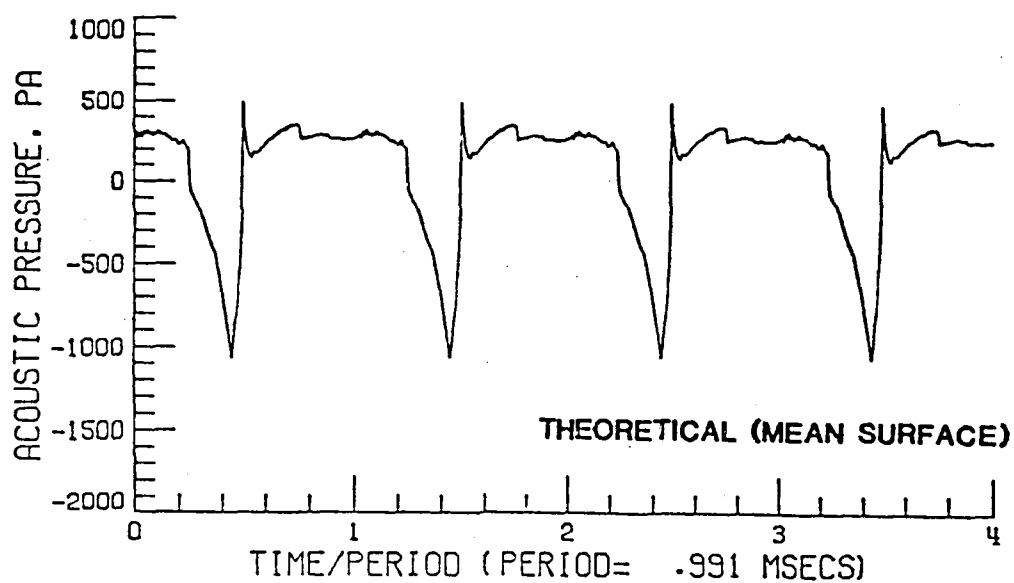
Figure 17.— Comparison of measured and predicted acoustic pressure signatures and spectra at microphone 4. Boom reflection correction included.
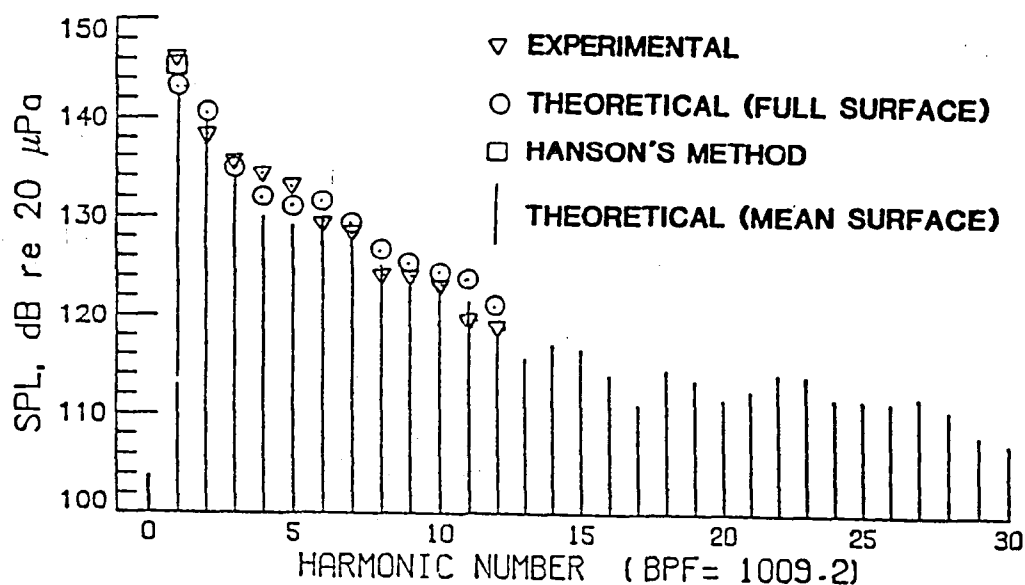
Figure 18.- Predicted acoustic pressure signature and spectrum at microphone 4 using mean surface calculations. Boom reflection correction included.

Standard Bibliographic Page

1. Report No. NASA TM-88993	2. Government Accession No.	3. Recipient's Catalog No.
4. Title and Subtitle Advanced Turboprop Noise Prediction-Development of a Code at NASA Langley Based on Recent Theoretical Results		5. Report Date July 1986
		6. Performing Organization Code 535-03-11
7. Author(s) F. Farassat, M. H. Dunn, S. L. Padula		8. Performing Organization Report No.
9. Performing Organization Name and Address NASA Langley Research Center Hampton, VA 23665-5225		10. Work Unit No.
		11. Contract or Grant No.
12. Sponsoring Agency Name and Address National Aeronautics and Space Administration Washington, DC 20546-0001		13. Type of Report and Period Covered Technical Memorandum
		14. Sponsoring Agency Code

15. Supplementary Notes   F. Farassat and S. L. Padula, NASA Langley Research Center Hampton, VA; M. H. Dunn, PRC Kentron, Inc., Hampton, VA
Paper presented at the 9th AIAA Aeroacoustics Conference, Williamsburg, Virginia, October 1984, "The Unified Acoustic and Aerodynamic Prediction of Advanced Propellers in the Time Domain," AIAA Paper 84-2303.

16. Abstract

    This paper is on the development of a high speed propeller noise prediction code at Langley Research Center. The code utilizes two recent acoustic formulations in the time domain for subsonic and supersonic sources. The selection of appropriate formulation is automatic in the code. The structure and capabilities of the code are discussed. Grid size study for accuracy and speed of execution on a computer is also presented. The code is tested against an earlier Langley code. Considerable increase in accuracy an speed of execution are observed. Some examples of noise prediction of a high speed propeller for which acoustic test data are available are given. A brisk derivation of formulations used is given in an appendix

17. Key Words (Suggested by Authors(s)) advanced turboprop, noise prediction, supersonic sources, computer code	18. Distribution Statement Unclassified – Unlimited Subject Category – 71

19. Security Classif.(of this report) Unclassified	20. Security Classif.(of this page) Unclassified	21. No. of Pages 57	22. Price A04

For sale by the National Technical Information Service, Springfield, Virginia 22161

NASA Langley Form 63 (June 1985)